Please cite this article in press as: Orr et al., Mapping the distribution and affinities of ligand interaction sites on human serum albumin, Biophysical Journal (2025), https://doi.org/10.1016/j.bpj.2025.03.016

Biophysical Journal
Article

Biophysical Society

Mapping the distribution and affinities of ligand interaction sites on human serum albumin

Asuka A. Orr,[1,2] Agbo-Oma Uwakweh,[1] Xun Li,[1] Ahmad Kiani Karanji,[1] Stephen W. Hoag,[1] Daniel J. Deredge,[1,*] and Alexander D. MacKerell, Jr.[1,*]

[1]Department of Pharmaceutical Sciences, School of Pharmacy, University of Maryland Baltimore, Baltimore, Maryland and [2]SilcsBio LLC, Baltimore, Maryland

ABSTRACT Ligands in many instances interact with a protein at multiple sites with a range of affinities. In this study, ligand-protein interaction sites on human serum albumin (HSA) are mapped using the site-identification by ligand competitive saturation (SILCS)-Biologics approach in conjunction with hydrogen-deuterium exchange (HDX)-mass spectrometry (MS) experiments. Ligands studied include known HSA binders, ibuprofen and ketoprofen, and compounds arginine, alanine, sucrose, and trehalose, excipients used in therapeutic formulations of protein-based drugs. In addition, the impact of excipient binding to HSA on its stability is investigated through temperature-ramp stability studies monitoring solution viscosity. For the studied ligands, interactions that correspond to known drug-binding sites (DSs) are identified. These include previously identified ibuprofen and ketoprofen interaction sites as well as additional sites and, in the case of the excipients, the ligands are shown to also bind at previously unidentified interaction sites, termed excipient sites (ESs) with 20 or more sites identified for the studied compounds. HDX-MS titrations were used to determine dissociation constants for a subset of the interaction sites for ibuprofen, ketoprofen, arginine, and sucrose, which exhibited K_d values in the low micromolar to millimolar range in satisfactory agreement with SILCS-Biologics predicted affinities, validating the computational approach to identify both high- and low-affinity interaction sites. The stability studies indicate the excipients offer protection at low excipient/protein ratios up to 66 with destabilization occurring at ratios above 132 with the exception of sucrose at the t_0 time point, indicating that the more favorable affinities of sucrose seen in the SILCS-Biologics and HDX-MS analyses contribute to protein stabilization. These results indicate that ligands can bind to large numbers of interaction sites on proteins, with those interactions having implications for the development of formulations for therapeutic proteins.

SIGNIFICANCE Ligand binding to proteins influence their biological function and stability with implications for therapeutic outcomes. Using a combination of experimental and computational ligand-protein mapping, it is shown that several ligands, including the drugs ibuprofen and ketoprofen and the excipients arginine and sucrose, bind to multiple sites on human serum albumin. The presence of excipients binding at these sites is shown to impact protein stability, indicating the importance of multiple interaction sites for the formulation of protein-based drugs.

INTRODUCTION

Low-affinity interactions of small molecules and solutes to proteins play a vital role in their function by stabilizing their folded native state and mediating their dynamic reversible interactions with other macromolecules crucial for biological processes such as signaling, regulation, and metabolism. These transient interactions allow proteins to respond to environmental changes, mediate allosteric regulation, and engage in cooperative binding. In drug discovery, low-affinity molecules identified in fragment-based approaches represent low-molecular-weight (MW) weak binders that can be optimized into more potent therapeutics, while also reducing the risk of off-target effects and toxicity (1–6). In biologics formulations, excipients are inactive ingredients, often of low MW, in pharmaceutical formulations that may exhibit low-affinity binding characteristics. Excipients can weakly interact with the protein therapeutic, typically forming transient, excipient-protein interactions that enhance drug stability and solubility by stabilizing the protein's active structure and blocking protein-protein interactions (PPIs) (7–10).

Submitted November 30, 2024, and accepted for publication March 20, 2025.

*Correspondence: dderedge@rx.umaryland.edu or alex@outerbanks.umaryland.edu

Editor: Abhishek Singharoy.

https://doi.org/10.1016/j.bpj.2025.03.016

Please cite this article in press as: Orr et al., Mapping the distribution and affinities of ligand interaction sites on human serum albumin, Biophysical Journal (2025), https://doi.org/10.1016/j.bpj.2025.03.016

Mapping and quantitating low-affinity interactions between low MW ligands and proteins presents several inherent challenges due to the transient and weak nature of these interactions. Characterizing such interactions is further complicated by the possibility and likelihood that small molecules may interact with multiple sites on a protein and the protein structure is flexible and may change in response to those interactions. X-ray crystallography, NMR, and cryogenic electron microscopy can provide detailed, atomic resolution of molecular interactions including ligand-protein interactions; however, these techniques cannot reliably detect low-affinity interactions due to the low occupancy nature of the interactions and are incapable of quantitatively assessing binding affinity (11–15). Various spectroscopic or calorimetric approaches may also detect the low-affinity interaction of small molecules with proteins; however, these techniques often lack the ability of identifying and mapping the site(s) of interaction (16–20).

Hydrogen-deuterium exchange mass spectrometry (HDX-MS) is a powerful technique for studying conformational properties of proteins, protein folding, protein aggregation, protein-ligand interactions, and therapeutic protein formulations (21–25). After exposure to a solution made with deuterated solvent (^2H_2O or D_2O), HDX-MS measures the exchange of hydrogen for deuterium atoms at the amide hydrogens of the protein's backbone, leading to an increase in mass as a function of exposure to deuterium-containing solvent (26). After deuterium exchange, the protein is digested into peptide fragments by acid proteases and the shifts in peptide mass due to deuterium uptake are detected by MS. Typically, when a ligand binds to a protein, it can result in the direct protection from deuterium exchange at the interaction site. In addition, protein-ligand interactions can also alter the protein's local structural dynamics, resulting in further protection or local deprotection from deuterium exchange. Thus, comparing deuterium uptake between a protein in the presence and absence of a small molecule can provide insights into where the ligand is binding. For high-affinity ligands, HDX-MS has been widely used to map protein-ligand interactions (27–31) and even model protein-ligand poses with high structural resolution (32). Additionally, HDX-MS has also been successfully applied in a quantitative approach to estimate global and localized dissociation constants by monitoring deuterium exchange as a function of ligand concentration (33–35). For low-affinity interactions, HDX-MS has been shown to be uniquely suitable for the simultaneous qualitative assessment of multiple localized effects resulting from transient, weak interactions with excipients, salts, additives or preservatives, in particular in the context of therapeutic antibodies, and providing structural insights of aggregation-inducing PPIs (36–42). However, extracting atomic-level 3D structural information or atomic-resolution information of low-affinity small-molecule ligand-protein interactions from such HDX-MS data remains a challenge.

Computational approaches such as molecular dynamics (MD) simulations and free-energy calculations have been used to resolve uncertainties or complement insights from experimental data by elucidating the mechanisms of protein-ligand interactions (43–47), among others. Such simulation methods have been successfully used to integrate data from HDX experiments to refine 3D structures of proteins (48–52). With respect to identifying multiple ligand-binding sites a number of methods have been presented (53–56). Of these, the site-identification by ligand competitive saturation (SILCS) method is a computational cosolute sampling approach that has been shown to be of particular utility for the identification of potential binding sites on a protein (57,58). In the SILCS approach, the interaction of the protein with multiple solutes, representing different functional groups, and water are sampled with a combination of Grand Canonical Monte Carlo (GCMC) and MD simulations. The functional group probability distributions in and around the protein are extracted from the SILCS simulations to build 3D grid free energy (GFE) binding maps (FragMaps), which may be used for qualitative inspection of functional group interaction patterns as well as provide the basis for quantitative analyses including small-molecule docking (58,59), ligand optimization (60), hotspots identification (61,62), pharmacophore modeling, and for calculation of PPIs (63). The SILCS-Biologics approach (64,65) builds on the SILCS technology for the rational selection of excipients for biologics formulations. In the SILCS-Biologics approach, SILCS simulations are first performed to generate FragMaps of a target macromolecule. These FragMaps are then used to predict regions of a protein prone to participate in PPI and map all possible interaction sites of small molecules including buffers and excipients, including low-affinity interactions (64–68). This information may then be used to identify protein formulations that maximize protein stability and limit PPI thereby lowering viscosity and aggregation rates (66,68).

Here, we combine HDX-MS, SILCS-Biologics, and formulation stability studies to map the multiple interactions occurring between small molecules and a model protein, human serum albumin (HSA), and understand how these interactions affect HSA stability. HSA is a plasma protein that binds and facilitates the vascular transport of diverse compounds including drugs, hormones, metal ions, and metabolites, functions that lead to it being used in the clinic (69). The promiscuous binding of HSA is largely the result of the presence of several "drug-binding sites" (DSs) (Fig. 1). While HSA drug sites DS 1 and DS 2 (Sudlow sites I and II) (71–73) were historically expected to be the primary binding sites of HSA, several structural studies of HSA and other mammalian serum albumins have revealed additional DSs (Fig. 1) (74–81).

Please cite this article in press as: Orr et al., Mapping the distribution and affinities of ligand interaction sites on human serum albumin, Biophysical Journal (2025), https://doi.org/10.1016/j.bpj.2025.03.016

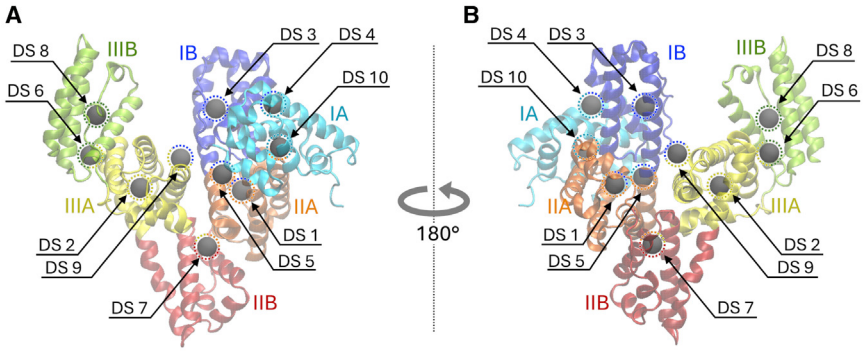

FIGURE 1 Locations of binding sites in HSA reported in previous studies reviewed in (70). Drug-binding sites (DSs) are shown as black spheres. HSA is shown in cartoon representation and colored by subdomains. Domains are labeled with Roman numerals (I, II, and III), and subdomains are labeled with letters (e.g., IA).

In the present study, SILCS-Biologics is used to identify possible ligand-protein interactions throughout HSA in conjunction with HDX-MS experiments. Furthermore, HDX-MS data are used to measure localized dissociation constants (K_d) in the μM to mM range of the small molecules allowing for validation of both the interaction site locations and affinities predicted by SILCS-Biologics, termed ligand grid free energies (LGFEs). The effect of low-affinity small-molecule binding on HSA stability is then evaluated with accelerated formulation stability studies that examine the thermodynamic and colloidal stability of HSA (68,82). The SILCS-Biologics metrics provide insights into the mechanisms that alter the stability of HSA induced by the presence of different types of excipients. Our study shows that HSA has multiple interaction sites for both known compounds and excipients, including previously unidentified low-affinity sites as well as how the information content from SILCS-Biologics can be used to facilitate formulation optimization.

MATERIALS AND METHODS

HDX-MS methods

Protein, ligand, and excipient preparation

A stock solution of HSA (Sigma-Aldrich, Darmstadt, Germany, A9511) was prepared by dissolving 66 mg in 5 mL of 1× PBS solution to make a 200 μM stock. This solution was aliquoted into 1 mL portions and stored in a −20°C freezer. To prepare an aliquot for HDX-MS, size-exclusion chromatography was performed using a Cytiva AKTA pureM purification system with a Superdex 200pg HiLoad preparative column. The eluted peak corresponding to the HSA protein was collected and concentrated to approximately 171 μM using an Amicon Ultra15 Centrifuge tube (UFC901024, 10K, NMWL 10,000). The concentration was monitored using a Nanodrop UV-vis Spectrophotometer.

Ibuprofen (Sigma-Aldrich, I4883) stock solutions were prepared at an initial concentration of 10 mM in 1× PBS:1% DMSO. This solution was then diluted to 1 mM and used to prepare the HSA-ligand solutions. HSA samples were prepared at a concentration of 20 μM in 1× PBS:1% DMSO either in the absence or with varying concentrations of ibuprofen (750, 500, 250, 100, 50, 25, or 10 μM). Ibuprofen stock solution in deuterium was prepared at an initial concentration of 10 mM stock solution in 10× PBS in D_2O and 1% DMSO and diluted to 1 mM in 1× PBS in D_2O and 1% DMSO. The ibuprofen concentrations (750, 500, 250, 100, 50, 25, or 10 μM were prepared at 1× PBS in D_2O, 1% DMSO, and the pD was adjusted to 7.4 using 0.1 N DCl.

Ketoprofen (Sigma-Aldrich, I1751) stock solutions were prepared at an initial concentration of 10 mM in 1× PBS:1% DMSO. This solution was then diluted to 1 mM and used to prepare the HSA-ligand solutions. HSA samples were prepared at a concentration of 20 μM in 1× PBS:1% DMSO either in the absence or with varying concentrations of ibuprofen (750, 500, 250, 100, 50, 25, 15, or 10 μM). Ketoprofen stock solution in deuterium was prepared at an initial concentration of 10 mM in DMSO and diluted to 1 mM in 1× PBS:1% DMSO in D_2O. The ketoprofen concentrations (750, 500, 250, 100, 50, 25, 15, or 10 μM, Apo) were prepared at 1× PBS in D_2O, 1% DMSO, and the pD adjusted to 7.4 using 0.1 N DCl.

All excipient compounds were purchased from Sigma-Aldrich. Stock excipient solutions of sucrose, trehalose, and alanine were prepared at a concentration of 1 M in 1× PBS in H_2O or D_2O. Arginine was prepared at 800 mM. The pH was adjusted to 7.4 for the H_2O buffer with either HCL or NaOH. The deuterium stock solutions were adjusted to a pD of 7.4 with either DCl or NaOD. Protein working solutions were prepared by making 100 μL of 20 μM protein in 1× PBS with the excipient concentrations at 10, 20, 50, 100, 250, and 500 mM of excipient. Deuterium buffer working solutions were prepared by making 200 μL of 10, 20, 50, 100, 250, and 500 mM of excipient in 1× PBS in D_2O. The pD was adjusted to 7.4. Solutions were stored at −20°C until the HDX-MS experiment. Excipient concentrations at 5, 1, and 0.1 mM were also prepared for sucrose and arginine to extend the concentration range probed for these excipients points into the micromolar concentration range.

HDX-MS

Before HDX-MS labeling experiments, a sequence coverage map was first obtained by analyzing undeuterated protein in the following manner: 2 μL of the 20 μM protein in 1× PBS was diluted with 18 μL of 1× PBS and mixed with 60 μL of ice-cold quench solution (8 M urea and 200 mM TCEP in 100 mM glycine solution [pH 2.5]). After a 3 min hold, the solution was diluted further with 170 μL of 100 mM glycine (pH 2.5) before injection.

For ibuprofen and ketoprofen, HDX reactions were performed by diluting 2 μL of the 20 μM protein sample in the absence or presence of a given compound at the concentrations listed above with 18 μL of the corresponding deuterium labeling solution and allowed to react for 1000 s at room temperature (25°C). Subsequently, the samples were immediately quenched on ice using 60 μL of the ice-cold quench solution (8 M urea, 200 mM TCEP, 100 mM glycine solution [pH 2.5]). After a 3 min hold, the samples were diluted with 170 μL of 100 mM glycine (pH 2.5) solution and analyzed before injection into a Waters NanoAcquity UPLC HDX system coupled to a Waters Synapt G2S Mass Spectrometer. Reactions were performed in triplicates.

For excipients, HDX reactions were performed by diluting 1 μL of protein working solution with or without a given excipient at the concentrations listed above with 9 μL of corresponding deuterium labeling

Please cite this article in press as: Orr et al., Mapping the distribution and affinities of ligand interaction sites on human serum albumin, Biophysical Journal (2025), https://doi.org/10.1016/j.bpj.2025.03.016

solution at room temperature. The reactions were performed for 10, 100, or 1000 s. The reaction mixtures were then quenched on ice by adding 70 μL of ice-cold quench solution (8 M urea, 500 mM TCEP, 100 mM glycine [pH 2.5]), for 5 min and diluted by adding 170 μL 500 mM TCEP in 100 mM glycine (pH 2.5) before injection into a Waters M-class UPLC HDX system coupled with a Waters Synapt G2Si mass spectrometer. Reactions were performed in triplicates.

HDX-MS data acquisition and processing was performed as previously described (31,83,84). In brief, in-line pepsin digestion was performed using either a pepsin column purchased from NovaBioAssays (excipient samples and respective controls) or an in-house packed pepsin column (ibuprofen, ketoprofen, and respective controls). The resulting peptides were separated using an Acquity UPLC BEH C18 column and eluted into the mass spectrometer. To elute the peptides, a 7 min, 5–35% acetonitrile (0.1% formic acid) gradient was utilized. MS data were acquired in MSe mode at the following settings: 20–30 V ramp trap CE and a continuous lock Mass (leucine-enkephalin) for mass accuracy correction. For sequence coverage analysis, peptide identification was performed using Protein Lynx Global Server 3.0.3 (PLGS) to obtain a peptide list. Peptides were further filtered using DynamX 3.0 Software (Waters, Milford, MA, USA) with a filter of 0.3 fragments ions per residue. DynamX was used to analyze the centroid mass shift of peptide isotopic envelops and track the uptake of deuterium for the peptide fragments as a function of deuterium labeling time for each condition.

Derivation of local equilibrium dissociation constant from HDX-MS data

The difference in deuterium uptake as a function of ligand or excipient concentration was used as a signal to monitor local protein/ligand or protein/excipient interactions at a peptide level spatial resolution. For that purpose, the difference in deuterium uptake ($\Delta D_{t,x}$) between a given condition x (in the presence of ligand or excipient at a given concentration) and a control (in the absence of ligand or excipient) at a given HDX reaction time t was calculated for each individual peptide fragment. Negative $\Delta D_{t,x}$ values correspond to regions of deprotection, and positive $\Delta D_{t,x}$ values correspond to regions of protection on the protein. OriginPro 2021b software was used to generate plots of $\Delta D_{t,x}$ versus ligand or excipient concentration and derive localized dissociation constant values by fitting to the following equation:

$$\Delta D_t = \frac{\Delta D_{t,x}^{\max} \cdot [X]}{[X] + K_d}$$

where $\Delta D_{t,x}^{\max}$ is the fitted maximal amplitude in difference in deuterium uptake, $[X]$ is the concentration of ligand or excipient, and K_d is the derived localized equilibrium dissociation constant value. For a given condition (ligand or excipient), confidence intervals (98% CI) in $\Delta D_{t,x}$ were calculated using a pooled standard error in deuterium uptake across all deuterium labeling time points and concentrations. A selection criterion was applied where a K_d is accepted if at least two $\Delta D_{t,x}$ data points in a $\Delta D_{t,x}$ versus $[X]$ plot are outside the calculated 98% CI. The binding affinity of the ligands/excipients at sites with apparent K_d values below the lowest concentration used (10 μM for ibuprofen and ketoprofen, or 0.1 mM for sucrose and arginine) may be underestimated due to limitation in experimental resolution.

Accelerated stability

The stability study took samples at t_0 (initial) and t_1 (7 days). Storage conditions were aligned with ICH guidelines for room temperature conditions, maintaining a temperature of 25°C and a relative humidity of 60%. At each time point, Tm (described below) and visual inspection for precipitation were assessed. The formulations were placed in dram amber glass vials (type 1 borosilicate glass) with black polypropylene caps for storage.

Viscosity measurement and Tm determination

An accelerated stability study was conducted to evaluate the stability of HSA at concentrations of 125, 250, and 500 mg/mL in the presence of sucrose, arginine, alanine, and trehalose. The study was performed using a Discovery HR-2 Rheometer equipped with a 40.0 mm parallel plate geometry and a Peltier stainless steel plate (serial no. 109595) to ensure precise rheological measurements. The experiment was conducted under controlled conditions, with the temperature starting at 10°C and increasing to 80°C at a ramp rate of 2°C/min. The measurements were taken at a constant shear rate of 50 s^{-1}, with each sample volume set at 0.2 mL. The stability was assessed at two time points: t_0 (initial) and t_1 (1 h after t_0) under an accelerated condition of 55°C.

As discussed in Xun and coworkers, the temperature viscosity profile consists of some initial changes in viscosity due to localized confirmational changes that affect PPI; these baseline shifts were taken as the pre-Tm. These baseline shifts were followed by a substantial change in viscosity due to global protein denaturation; this shift was taken as Tm (68). Typically there was zero or one baseline shift that exceeded the baseline noise level. Thus, we only analyzed baseline shifts that exceeded the baseline noise level; in all cases these baseline shifts were the shifts immediately before the Tm. Viscosity data after the Tm were not analyzed as this information is not relevant to protein stability. From these viscosity profile curves the melting temperature (Tm) for each viscosity profile was determined by calculating the inflection point of the pre-Tm (ΔPreTm) and primary Tm (ΔTm) from the rheological temperature scan (68).

The viscosity versus temperature data were imported into MATLAB, where a custom script was used to smooth the data. Fitting the data was a two-step process; first the MATLAB built in function "smoothdata" was used to smooth the data. This function uses a moving average; for each element of the viscosity vector, it calculates an average value in the window around that element. Then the window slides down the length of the vector, computing an average over the elements within each window. In terms of data fitting, the smoothdata function requires two parameters, the averaging method and window size. To determine the best combination of these parameters, a MATLAB script was developed to fit all the data for each averaging method and a range of window sizes, the root mean-square error was then computed, and a residual plot for each viscosity profile was plotted. The analysis found that the quadratic regression over a window of 30 data points was the best averaging method. We then used the MATLAB gradient function to calculate the second derivative and determined when the second derivative equals zero. This analytical approach allowed for a precise assessment of the thermal and rheological stability of the samples. These methods are described in detail by Xun and co-workers (68).

Computational methods

SILCS simulations and FragMap construction

The SILCS-Biologics approach uses precomputed FragMaps, constructed from SILCS simulations, to map ligand or excipient binding sites and regions prone to protein-protein interaction. FragMaps of HSA were derived in our previous study involving the prediction of protein effective charge in different salt environments (67). In brief, SILCS simulations were performed to sample the interaction of solutes representing different functional groups and water with HSA. The initial coordinates of HSA were extracted from the crystal structure of HSA (PDB: 4K2C (85)). The SILCS simulations consist of 10 independent runs that include GCMC calculations in which the excess chemical potential (μ_{ex}) of both the solute and water molecules are oscillated to attain their target concentrations in the simulation system followed by GROMACS (86) energy minimization and MD simulations. The workflow was performed using the SILCS software suite, version 2022 (SilcsBio, Baltimore, MD, USA). Upon completion of the SILCS simulations, an aggregate 1 μs of simulation trajectories (10 GCMC/MD simulations of 100 ns each) was generated with simulation snapshots saved

Please cite this article in press as: Orr et al., Mapping the distribution and affinities of ligand interaction sites on human serum albumin, Biophysical Journal (2025), https://doi.org/10.1016/j.bpj.2025.03.016

every 10 ps. Using the resulting simulation snapshots, probability distributions of the solute and water molecules in and around HSA were calculated to produce FragMaps. The FragMaps correspond to the normalized probability distributions of selected solute atoms and water oxygens on a 1 $Å^3$ grid. The probability distributions are normalized based on the concentrations of the solute and water in aqueous solution alone and the number of atoms in the solutes used to define a given FragMap type. The normalized probability FragMaps are converted into free energies based on a Boltzmann transformation to yield GFEs for subsequent qualitative and quantitative analysis.

The FragMaps are the basis for subsequent SILCS methods, including SILCS-MC docking (58,59), for which the binding affinity of a docked pose is estimated by the LGFE. The LGFE is based on the summation of the GFE scores for the classified atoms in each ligand. The atomic GFE scores are determined by the overlap of each ligand atom with a specific FragMap as defined by the atom classification scheme described in the supporting material (Fig. S1). In the SILCS-MC docking, the protein structure is also implicitly accounted for through the SILCS Exclusion Map. The SILCS Exclusion Map occupies those regions of system space where no solute or water molecule nonhydrogen atom sampling occurred during the entirety of the SILCS simulations. During the docking a large unfavorable energy penalty is imposed if there is an overlap of a ligand atom with the Exclusion Map. Additional details on the generation of HSA FragMaps used in this study are provided in (67). The SILCS simulation procedure is described in detail in (60,87) and the procedure to generate SILCS FragMaps and GFEs is described in detail in (60).

SILCS-Biologics ligand interaction site identification

The SILCS-Biologics approach systematically maps ligand-protein interactions, enabling high-throughput in silico screening of single and combinations of ligands, including excipients for biologics formulation. In addition, the PPI interaction pattern of a protein with itself may be mapped. In the case of protein formulation, in which excipients are identified to stabilize the protein and minimize aggregation and viscosity, these capabilities allow for the identification of the excipients that interact with sites of the protein that participate in PPI. To achieve this SILCS FragMaps are used in PPI docking and global docking of ligands on the protein surface through SILCS-PPI (63) and SILCS-Hotspots (61,62), respectively. In this study, global docking to HSA was performed for the drugs ibuprofen and ketoprofen, and for the excipients arginine, alanine, sucrose, and trehalose, as well as the buffer phosphate (1× PBS) using the SILCS-Hotspots portion of SILCS-Biologics. The poses of the docked compounds were then further refined using SILCS-MC docking from which the full distribution of ligand-protein interactions along with their predicted LGFE scores were obtained. Further details on SILCS-Hotspots and SILCS-MC docking are provided in the supporting material.

The refined binding poses were analyzed for their predicted binding free energies (LGFE), occupancy at different excipient concentrations, proximity to residues prone to intramolecular interactions and to intermolecular PPI, and percent relative buried surface area (%rBSA). The LGFE of each refined binding pose corresponds to the LGFE determined from SILCS-MC docking. The occupancy of an excipient in a given pose is calculated based on its LGFE and the experimental ligand concentration, with the maximum possible occupancy being 1 and the minimum possible occupancy being 0:

$$\text{occupancy} = \frac{[\text{ligand concentration}]}{[\text{ligand concentration}] + e^{\frac{\text{LGFE}}{RT}}} \quad (1)$$

In Eq. 1, R is the Boltzmann constant, and T is the absolute temperature.

Residues prone to intermolecular PPI were determined by SILCS-PPI (63) through the SILCS-Biologics framework. In this study the PPI are calculated for HSA with respect to itself. SILCS-PPI is based on the overlap of the FragMaps and probability distributions of selected functional groups in the protein with comprehensive sampling of PPI orientations being performed through a fast-Fourier transform scheme. Based on the top 2000 PPI orientations, individual residues in each protein were assigned a PPI probability score for subsequent analysis. Details of the SILCS-PPI method may be obtained from (63). Residues involved in intramolecular interactions were detected using the simulation snapshots extracted from the SILCS simulations of HSA and MDAnalysis (88,89). If a residue was involved in an intramolecular salt bridge, π-π, or cation-π interaction for 50% or more of the SILCS simulation snapshots, then the residue was considered to be involved in an intramolecular interaction. A SILCS-Biologics predicted pose was considered to be in proximity to a residue involved in intramolecular interactions if any nonhydrogen atom of the ligand was within 4.5 Å of any nonhydrogen atom of the residue.

Correlation analysis

SILCS-Biologics metrics were subjected to correlation analysis against experimental data extracted from the HDX-MS and accelerated stability studies. The HDX-MS-derived $\Delta D_{t,x}$ values for each individual peptide fragment were correlated with the SILCS-Biologics occupancy sum of all ligands or excipients predicted to bind to the individual peptide fragment. Occupancy sums are calculated based on the occupancy of all ligands or excipients with any nonhydrogen atom within 4.5 Å of any nonhydrogen residue atom in each peptide fragment. For ibuprofen and ketoprofen, $\Delta D_{1000s,750\mu M}$ values were correlated with SILCS-Biologics occupancy sums calculated at 750 μM. ΔD values derived at HDX reaction time 1000 s and 750 μM of ibuprofen or ketoprofen were used as the magnitude of ΔD values, which was greatest at these conditions. For arginine and sucrose, $\Delta D_{10s,100mM}$ values were correlated with SILCS-Biologics occupancy sums calculated at 100 mM as this excipient concentrations is commonly found in biologics formulations (90). ΔD values derived at a HDX reaction time 10 s for arginine and sucrose were used as these values were hypothesized to represent the initial binding of the excipients and minimize the effects of local unfolding induced by the excipients. The HDX-MS-derived K_d values of the ligands and excipients for individual peptide fragments were converted to binding free energies ($\Delta G = RT\ln K_d$) and correlated with the LGFEs of the most energetically favored binding pose of the ligand or excipient for the corresponding individual peptide fragments. As individual peptide fragments may encompass similar sequence ranges (e.g., one peptide encompasses residues 395–407 and another peptide encompasses residues 395–408), the peptide acquiring the most favorable HDX-MS-derived K_d value is used in the correlation and the K_d value of the overlapping peptide is omitted from the correlation. All T_m and $PreT_m$ values derived from the accelerated stability studies were correlated with all SILCS-Biologics metrics to identify which metrics are most predictive of excipient-induced HSA stabilization or destabilization.

RESULTS

Ligand-protein interactions represent a cornerstone of biophysics that is central to a range of biological processes as well as other phenomena including the development of both small-molecule and protein-based therapeutics. In this study we investigated the capability of a combined computational and experimental approach to comprehensively map the interactions and affinities of small molecules with the model protein HSA. This was initially performed with two known binders of HSA, ibuprofen and ketoprofen, to determine if the applied approach was able to identify known sites as well as identify previously unknown sites, including sites with lower affinity of the compounds on the protein. Subsequently, the method was applied to known excipients, arginine, alanine, sucrose, and trehalose, as the action of these compounds is based on the presence of both high- and

Please cite this article in press as: Orr et al., Mapping the distribution and affinities of ligand interaction sites on human serum albumin, Biophysical Journal (2025), https://doi.org/10.1016/j.bpj.2025.03.016

low-affinity interaction sites on proteins. The importance of this range of interactions is then shown through protein stability experiments indicating their effectiveness and offering possible mechanisms to explain their role in protein formulation. Together, the present results indicate that, with the model protein HSA, there exists multiple interaction sites with a range of affinities and that such sites on therapeutic proteins can be exploited for protein formulation.

Identification of crystal-resolved and previously unresolved ibuprofen and ketoprofen binding sites

To assess the interactions of ibuprofen and ketoprofen with HSA, HDX-MS was acquired in the absence and the presence of increasing concentrations of ligands. Fig. 2 *A* (ibuprofen) and 2B (ketoprofen) show the difference in deuterium uptake observed after 1000 s of deuterium incubation ($\Delta D_{1000s,x}$) at various concentrations of ligand (from 10 to 750 μM) versus the absence of ligand for all peptides identified. The difference plots show regions of significant, ligand concentration-dependent protection throughout HSA for both ligands. In addition, both ligands are also seen to induce significant deprotection in few localized regions of HSA. SILCS-Biologics was performed and correlated with HDX-MS data to identify the range of interaction sites of ibuprofen and ketoprofen on HSA. In simple terms, the protection/deprotection from deuterium uptake may be related to the number of interaction sites in the

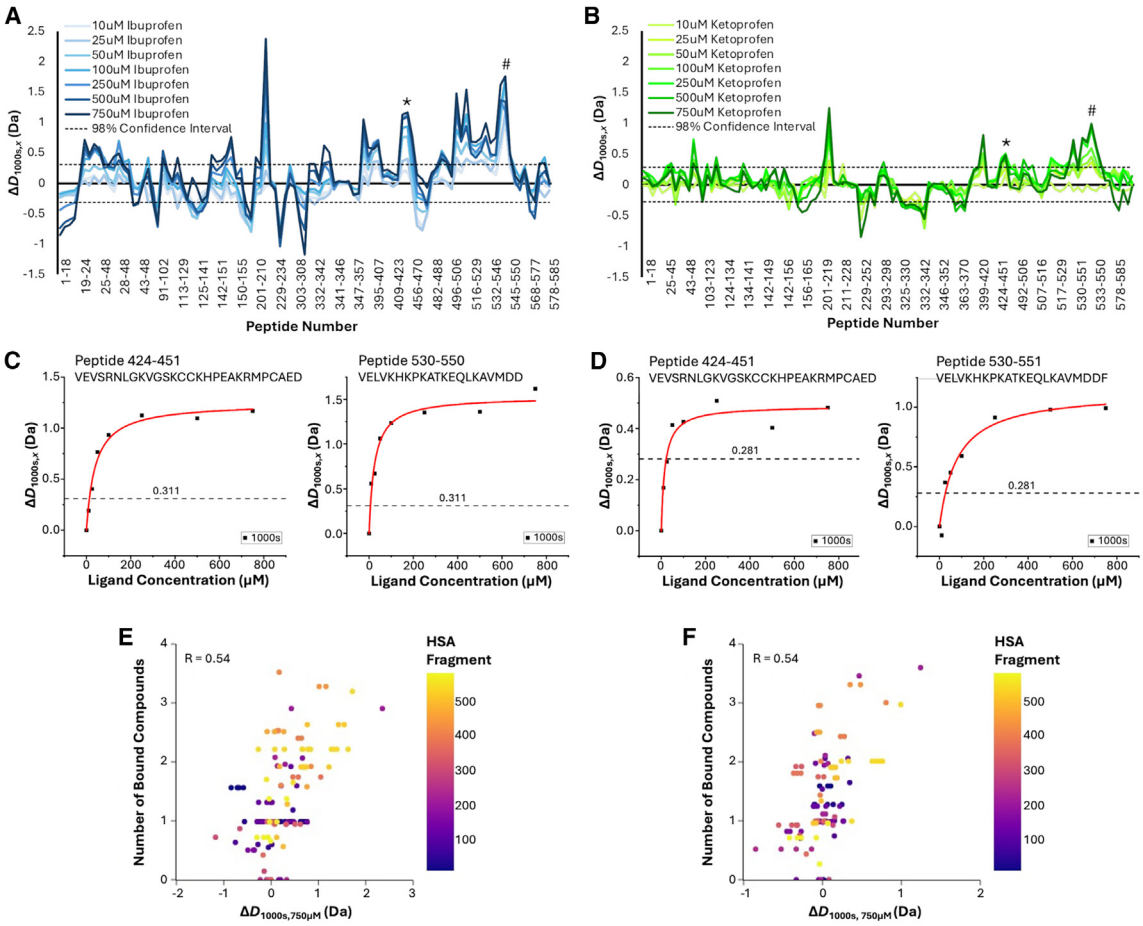

FIGURE 2 HDX-MS shows ligand-induced changes in deuterium uptake correlating with the SILCS-Biologics metric, number of bound ligands. The difference plots for deuterium uptake after 1000 s ($\Delta D_{1000s,x}$) reaction of HSA in PBS minus HSA in PBS supplemented with various concentrations of (*A*) ibuprofen and (*B*) ketoprofen. Individual peptide fragments are listed on the *x* axis from the N- to the C-terminus. $\Delta D_{1000s,x}$ values for each HSA peptide fragment were calculated as the deuterium uptake of the peptide fragment in the absence of ligand minus the deuterium uptake of the peptide fragment in the presence of ligand. Thus, positive values indicate that the ligand protects the peptide from deuteration, and negative values indicate that the ligand deprotects the peptide from deuteration. A representative peptide of crystallographically resolved drug site 2 is shown as (*) and the difference in deuterium uptake as a function of ligand concentration is shown in (*C*, *left*) and (*D*, *left*). A representative peptide of additional drug site is shown as (#) and the difference in deuterium uptake as a function of ligand concentration is shown in (*C*, *right*) and (*D*, *right*). The correlation of the SILCS-Biologics metric, number of bound ligands (*y* axis) to HDX-MS-derived $\Delta D_{1000s,750\mu M}$ for individual HSA peptide fragment (*x* axis) is shown for (*E*) ibuprofen and (*F*) ketoprofen. The number of bound ligands per peptide fragment were calculated as the sum of occupancies of all compounds interacting with the given peptide. Each data point is colored based on the location of the corresponding peptide in the full-length HSA sequence, with blue corresponding to the N-terminus of HSA, and yellow corresponding to the C-terminus of HSA.

Please cite this article in press as: Orr et al., Mapping the distribution and affinities of ligand interaction sites on human serum albumin, Biophysical Journal (2025), https://doi.org/10.1016/j.bpj.2025.03.016

vicinity of a given peptide fragment. Based on SILCS-Biologics, ibuprofen and ketoprofen occupy 22 and 21 sites with an occupancy greater than 0.5 at the highest HDX-MS ligand concentration of 750 μM and 2 and 3 sites at the lowest HDX-MS ligand concentration of 10 μM. Correlation analysis of the HDX-MS-derived $\Delta D_{1000s,750\mu M}$ of HSA peptide fragments to SILCS-Biologics metric, the number of excipients bound in the vicinity of each fragment, shows fair correlations between the experimental and computational observations (R = 0.54 for both ibuprofen and ketoprofen, Fig. 2, *E* and *F*). Overall, HSA peptide fragments with high $\Delta D_{1000s,750\mu M}$, indicating that the presence of compounds protects the fragment from deuteration, are also predicted to be bound by a higher number of compounds (Fig. 2, *E* and *F*). In the few cases of deprotection, $\Delta D_{1000s,750\mu M} < -0.31$ for ibuprofen or $\Delta D_{1000s,750\mu M} < -0.28$ for ketoprofen, only a small number of compounds are interacting with the peptide, suggesting that the interaction leaves the majority of the peptide exposed and potentially structurally perturbed such that more exchange occurs. Overall, the reasonable agreement between SILCS-Biologics metrics and HDX-MS experiments indicates the utility of the SILCS-Biologics approach for the identification of ligand interaction sites on a protein regardless of the affinity of those sites.

Ibuprofen and ketoprofen have previously been experimentally determined to bind HSA (91–96). In accordance with previous x-ray crystallography studies (91,92), both HDX-MS and SILCS-Biologics show that ibuprofen binds to HSA DSs 2 and 7 and ketoprofen binds to HSA DSs 2, 3, and 9 (Fig. 2; Table 1; supporting material, hdx-ms_duptake.xlsx). SILCS-Biologics-derived LGFEs, which represent the ligands' binding free energies, of ibuprofen at sites 2 and 7 were −7.10 and −6.78 kcal/mol, respectively, and the LGFE of ketoprofen at sites 2, 3, and 9 were −7.28, −6.59, and −5.81 kcal/mol, respectively (Table 1). These LGFE's are in line with previous experimental studies reporting ibuprofen binding affinities to HSA ranging from 2.38 to 5.56 μM (−7.16 to −7.55 kcal/mol) and ketoprofen binding affinities to HSA ranging from 30 to 189 μM (−5.08 to −6.17 kcal/mol) (93–96). As previously demonstrated (33–35), the change in deuterium uptake as a function of ligand concentration can also be used to derive local binding affinities. Fig. 2, *C* and *D* display the $\Delta D_{1000s,x}$ versus ligand concentration of representative peptides for ibuprofen and ketoprofen, respectively. The resulting curve is fit to a single site binding isotherm to derive a dissociation constant, K_d (Table 1; supporting material, HDX_Ligand_Titrations_Figures.pptx). HDX-MS-derived affinities of ibuprofen to HSA peptides in proximity to DSs 2 and 7 were within the range of −4.97 to −6.54 kcal/mol and the affinities of ketoprofen to HSA peptides in proximity to DSs 2, 3, and 9 were in the range of −4.78 to −6.98 kcal/mol (Table 1; supporting material, HDX_Ligand_Titrations_Figures.pptx). Notably, the most favorable HDX-MS-derived affinities are also in line with previous experimental studies (93–96).

In addition to the crystal-resolved binding sites of ibuprofen and ketoprofen, both SILCS-Biologics and HDX-MS experiments detected the binding of both compounds at DSs 6 and 8 (Fig. 2; Table 1). The LGFEs of ibuprofen at DSs 6 and 8 were −4.28 and −6.51 kcal/mol, respectively. The LGFE of ketoprofen at DSs 6 and 8 were −7.31 and −6.13 kcal/mol, respectively. HDX-MS-derived affinities of the compounds to HSA peptides in proximity to DSs 6 and 8 were in the range of −4.67 to −7.27 kcal/mol for ibuprofen and −4.70 to −7.34 kcal/mol for ketoprofen (Table 1; supporting material, HDX_Ligand_Titrations_Figures.pptx). Notably, both the LGFEs and HDX-MS-derived affinities of the two compounds are within the same magnitude. Previous experimental and computational studies have suggested that HSA has several binding sites for ibuprofen and ketoprofen beyond those resolved in crystal structures (97–100), with the binding of ibuprofen to DSs 6 and 8 also detected in previous studies (96,101,102).

Beyond the strong interactions of ibuprofen at HSA DSs 2, 7, 6, and 8 and ketoprofen at sites 2, 3, 6, 8, and 9, additional sites at which the two drugs interact with HSA with lower affinity were predicted by SILCS-Biologics. These are shown in Fig. 3 as the space filling models not identified as being at the known DSs. Of those sites, those with occupancies >0.9 at 750 μM are shown as colored space filling while those with occupancy <0.9 are shown in transparent gray. For ibuprofen (Fig. 3 *A*), three additional higher occupancy sites are observed. One is between domains II and III and the other two are in domain I. With ketoprofen, three additional higher occupancy sites are observed, two of which are in domain II and one is in domain I. In addition, multiple interaction sites with low occupancies are observed for the two ligands. Many of these sites are located on peptides with substantial protection, $\Delta D_{1000s,750\mu M} > 0.25$, or deprotection, $\Delta D_{1000s,750\mu M} < -0.25$, identified in the HDX-MS experiments. Such sites were not amenable to K_d determination based on the HDX-MS results, but the present results indicate that SILCS-Biologics is able to identify sites where more transient binding can occur. This is notable as it indicates that small molecules likely have multiple, low-affinity interactions with proteins that are not accessible by direct experimental analyses, with those sites potentially being important for protein formulation as discussed below.

Detection of excipient interaction sites

Next, we extended our approach to study the interaction of HSA with lower-affinity excipients with expected K_d ranges in the high μM to mM range. HDX-MS was acquired in the absence and presence of increasing concentrations (100 μM–500 mM) of arginine and sucrose, two commonly found excipients. Fig. 4, *A* and *B* show the corresponding

Please cite this article in press as: Orr et al., Mapping the distribution and affinities of ligand interaction sites on human serum albumin, Biophysical Journal (2025), https://doi.org/10.1016/j.bpj.2025.03.016

TABLE 1 Affinities of ibuprofen and ketoprofen to HSA and individual HSA peptide fragments derived by SILCS-Biologics (LGFE) and HDX-MS (K_d and ΔG) and their association to HSA drug sites

Drug site	LGFE (kcal/mol)	Peptide fragment sequence	HSA residue range	K_d (μM)	ΔG (kcal/mol)
Ibuprofen					
DS 2	−7.10	AKVFDEFKPLVEEPQNL	371–387	62.50 ± 22.13	−5.73
		FEQLGEYKFQNAL	395–407	16.03 ± 4.56	−6.54
		FEQLGEYKFQNALL	395–408	16.94 ± 3.71	−6.51
		VEVSRNLGKVGSKCCKHPEAKRMPCAE	424–450	39.95 ± 6.99	−6.00
		VEVSRNLGKVGSKCCKHPEAKRMPCAED	424–451	39.92 ± 6.26	−6.00
DS 6	−7.46	FEQLGEYKFQNAL	395–407	16.03 ± 4.56	−6.54
		FEQLGEYKFQNALL	395–408	16.94 ± 3.71	−6.51
		LSEKERQIKKQTAL	516–529	10.98 ± 4.77	−6.76
		LSEKERQIKKQTALVE	516–531	11.03 ± 4.45	−6.76
		ALVELVKHKPKATKEQLKA	528–546	35.95 ± 13.30	−6.06
		VELVKHKPKATKEQLKAVMDD	530–550	24.37 ± 4.85	−6.29
		VELVKHKPKATKEQLKAVMDDFAA	530–553	4.65 ± 3.33	−7.27
		KAVMDD	545–550	9.30 ± 2.24	−6.86
DS 7	−6.78	ASLQKFGERAFKAWAVARL	201–219	226.13 ± 47.72	−4.97
DS 8	−6.65	TYVPKEFNAETFTFHADICTLSEKERQ	496–522	64.05 ± 9.54	−5.72
		LSEKERQIKKQTAL	516–529	10.98 ± 4.77	−6.76
		LSEKERQIKKQTALVE	516–531	11.03 ± 4.45	−6.76
		ALVELVKHKPKATKEQLKA	528–546	35.95 ± 13.30	−6.06
		VELVKHKPKATKEQLKAVMDD	530–550	24.37 ± 4.85	−6.29
		VELVKHKPKATKEQLKAVMDDFAA	530–553	4.65 ± 3.33	−7.27
		KAVMDD	545–550	9.30 ± 2.23	−6.86
		*AEEGKKLVA	*569-577	*379.11 ± 328.97	*-4.67
Ketoprofen					
DS 2	−7.28	*KPLVEEPQNL	*378-387	*82.99 ± 50.71	*-5.56
		FEQLGEYKFQNALL	395–408	40.23 ± 12.72	−5.99
		GEYKFQNALLVRYTKKVPQVST	399–420	55.87 ± 18.97	−5.80
		VEVSRNLGKVGSKCCKHPEAKRMPCAE	424–450	40.23 ± 17.68	−5.99
		VEVSRNLGKVGSKCCKHPEAKRMPCAED	424–451	16.43 ± 4.62	−6.52
DS 3	−6.59	LQHKDDNPNLPRLVRPEVDVM	103–123	128.07 ± 64.86	−5.31
		CTAFHDNEETFLKKYL	124–139	310.12 ± 296.86	−4.78
		*YAPELLF	*150-156	*7.55 ± 3.52	*-6.98
DS 6	−7.31	FEQLGEYKFQNALL	395–408	40.23 ± 12.72	−5.99
		GEYKFQNALLVRYTKKVPQVST	399–420	55.87 ± 18.97	−5.80
		VELVKHKPKATKEQLKAVM	530–548	96.88 ± 41.55	−5.47
		VELVKHKPKATKEQLKAVMDD	530–550	94.86 ± 37.20	−5.74
		VELVKHKPKATKEQLKAVMDDF	530–551	79.82 ± 24.25	−5.49
		ELVKHKPKATKEQLKA	531–546	46.40 ± 16.30	−5.91
		LVKHKPKATKEQLKA	532–546	61.80 ± 33.04	−5.47
		LVKHKPKATKEQLKAVM	532–548	59.35 ± 14.79	−5.74
		VKHKPKATKEQLKAVMDD	533–550	91.10 ± 35.42	−5.49
		KAVMDD	545–550	107.24 ± 31.25	−5.76
DS 8	−6.13	VELVKHKPKATKEQLKAVM	530–548	96.88 ± 41.55	−5.47
		VELVKHKPKATKEQLKAVMDD	530–550	94.86 ± 37.20	−5.74
		VELVKHKPKATKEQLKAVMDDF	530–551	79.82 ± 24.25	−5.49
		ELVKHKPKATKEQLKA	531–546	46.40 ± 16.30	−5.91
		LVKHKPKATKEQLKAVM	532–548	59.35 ± 14.79	−5.74
		VKHKPKATKEQLKAVMDD	533–550	91.10 ± 35.423	−5.49
		KAVMDD	545–550	107.24 ± 31.25	−5.76
DS 9	−5.81	VEVSRNLGKVGSKCCKHPEAKRMPCAE	424–450	40.23 ± 17.69	−5.99
		VEVSRNLGKVGSKCCKHPEAKRMPCAED	424–451	16.43 ± 4.62	−6.52

Peptide fragments deprotected by the presence of the ligands are denoted by *; all other peptide fragments were protected from deuteration. Drug sites in bold text correspond to sites identified in crystal structures. Peptide fragments may be associated with multiple drug sites. The binding affinities of the ligands at sites with apparent K_d values lower than 10 μM may be underestimations of the true binding affinity.

difference plots of arginine and sucrose, respectively, after 10 s of deuterium incubation. For clarity, concentrations between 10 and 500 mM are shown. A deuterium incubation time of 10 s was chosen after inspection of $\Delta D_{t,x}$ versus peptides at various time points (10, 100, and 1000 s) revealed that arginine largely results in deprotection at longer deuterium incubation time points of 100 and 1000 s (Fig. S2). Here again, the difference plots reveal regions of significant,

Please cite this article in press as: Orr et al., Mapping the distribution and affinities of ligand interaction sites on human serum albumin, Biophysical Journal (2025), https://doi.org/10.1016/j.bpj.2025.03.016

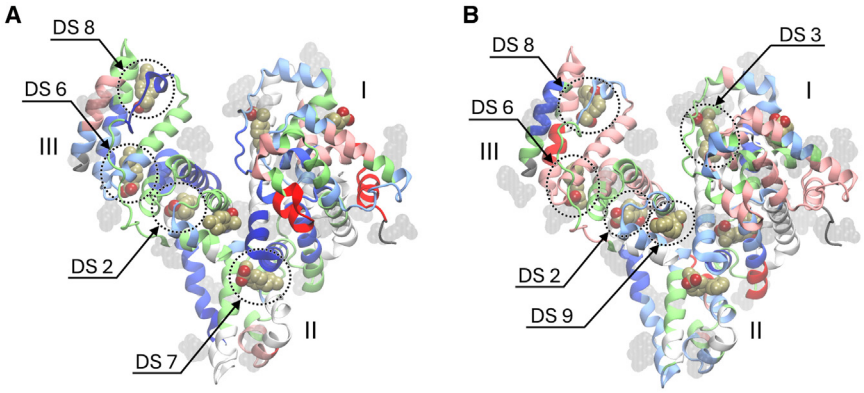

FIGURE 3 Interaction sites of (*A*) ibuprofen and (*B*) ketoprofen on HSA predicted by SILCS-Biologics and observed with HDX-MS experiments. Ibuprofen and ketoprofen compounds are shown in van der Waals representation. Ibuprofen and ketoprofen poses with occupancies predicted to be less than 0.9 by SILCS-Biologics are shown in transparent gray. HSA is shown in cartoon representation and is colored based on HDX-MS-derived $\Delta D_{1000s,750\mu M}$, with dark blue representing $\Delta D_{1000s,750\mu M} > 1$, blue representing $1 > \Delta D_{1000s,750\mu M} > 0.5$, light blue representing $0.5 > \Delta D > 0.25$, green representing $0.25 > \Delta D > -0.25$, light red representing $-0.5 < \Delta D_{1000s,750\mu M} < -0.25$, red representing $-1 < \Delta D_{1000s,750\mu M} < -0.5$, white representing residues not represented in the HDX-MS data, and gray representing flexible N- and C-termini.

excipient concentration-dependent protection throughout HSA for both excipients. Similarly, sucrose is also seen to induce a greater effect on deuterium uptake than arginine at $\Delta D_{10s,x}$, both in terms of amplitude of $\Delta D_{10s,x}$ and number of sites with significant effect. The interaction of excipients sucrose and arginine to HSA were next characterized using SILCS-Biologics and correlated with HDX-MS experiments. As observed above with ibuprofen and ketoprofen, correlation analysis of the HDX-MS-derived $\Delta D_{10s,100mM}$ of the HSA peptide fragments in the presence of the excipients to SILCS-Biologics metrics show fair correlations between the experimental and computational observations, with peptide fragments acquiring the highest $\Delta D_{10s,100mM}$ values also predicted to be bound by higher numbers of excipients ($R = 0.47$ for sucrose and $R = 0.53$ for arginine, Fig. 4, *E* and *F*). These results further indicate the consistency of the SILCS-Biologics and HDX-MS data with respect to range and location of interactions sites identified.

Consistent with the data in Fig. 4, SILCS-Biologics and HDX-MS indicate that both excipients interact with HSA at numerous sites (Fig. 5). Sucrose and arginine were predicted to occupy 33 and 47 sites with an occupancy greater than 0.5 at the highest HDX-MS excipient concentration of 500 mM, 22 and 11 sites at the HDX-MS excipient concentration of 100 mM, and 6 and 0 sites at the lowest HDX-MS ligand concentration of 0.1 mM, respectively. Mapping HDX-MS $\Delta D_{10s,100mM}$ onto the 3D HSA structure with SILCS-Biologics predicted poses of sucrose and arginine suggests specific interaction sites of the two excipients. Among the interaction sites high protection was observed in proximity to poses at DSs 1, 2, 4, 5, 6, and 9 for sucrose and DSs 8 and 10 for arginine (Fig. 5, *A* and *B*). Beyond the previously identified DSs of HSA (Fig. 1), additional interaction sites herein after referred to as excipient sites (ESs) were identified for the two excipients. Two excipient sites were identified for sucrose (Fig. 5 *A*, ES 1 and ES 2), and one excipient site was identified for arginine (Fig. 5 *B*, ES 3). Apart from sucrose poses acquiring more favorable LGFEs compared with arginine poses (supporting material, silcs-biologics_poses.xlsx, average LGFE of sucrose and arginine poses are −4.51 and −3.76 kcal/mol, respectively), the %rBSA of sucrose poses, including interactions predicted outside of the drug and excipient sites are higher than the arginine poses, indicating that sucrose binds in buried pockets of HSA whereas arginine primarily binds the surface of HSA (supporting material, silcs-biologics_poses.xlsx). Combined, the less energetically favorable LGFEs and lower %rBSAs of arginine poses suggest that arginine interactions to HSA are more transient than sucrose interactions, thereby reducing its ability to protect HSA from deuteration.

Interestingly, the $\Delta D_{10s,x}$ of HSA peptide fragments in the presence of sucrose are nearly all positive at $t = 10$ s, indicating that sucrose stabilizes all regions of HSA upon interaction (Fig. 5 *A*; supporting material, hdx-ms_duptake.xlsx). This is in line with previous studies showing that sucrose protects HSA from thermal and chemical denaturation (103,104). Additionally, $\Delta D_{t,x}$ values of HSA peptide fragments in the presence of sucrose at longer time points are also primarily positive, indicating that, even at longer interaction periods, sucrose still has an overall protective effect and induces minimal local unfolding (supporting material, hdx-ms_duptake.xlsx). Alternatively, the $\Delta D_{t,x}$ of HSA peptide fragments in the presence of arginine changes from generally positive to generally negative going from 10 to 1000 s (Figs. 5 *B*, 6 *A*, and S2; supporting material, hdx-ms_duptake.xlsx), with the correlation coefficient of the SILCS-Biologics Number of Bound Excipients metric to the $\Delta D_{t,x}$ changing to $R = -0.32$ at $t = 1000$ s. This indicates that arginine binding ultimately leads to deprotection after 1000 s. This may be due to it inducing some local unfolding of HSA thereby exposing more regions to the surrounding solvent and deuteration compared with HSA in the absence of arginine.

An attractive feature of SILCS-Biologics is the output of 3D structures of excipient locations on the target protein. As shown in Fig. 6 *A*, arginine led to destabilization to the majority of the structure of HSA at the HDX-MS

Please cite this article in press as: Orr et al., Mapping the distribution and affinities of ligand interaction sites on human serum albumin, Biophysical Journal (2025), https://doi.org/10.1016/j.bpj.2025.03.016

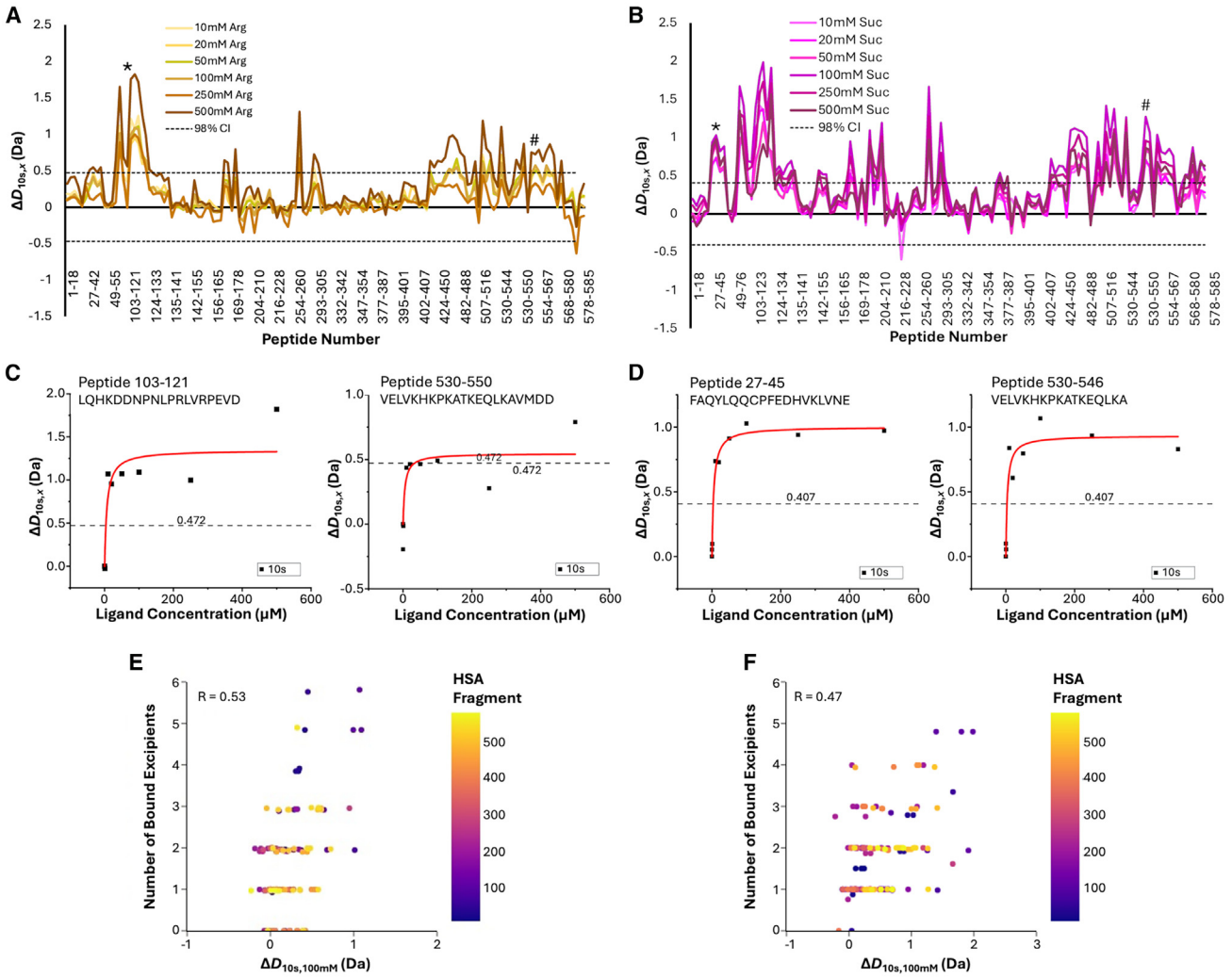

FIGURE 4 HDX-MS shows excipient-induced changes in deuterium uptake correlating with the SILCS-Biologics metric, number of bound ligands. The difference plots for deuterium uptake after 10 s ($\Delta D_{10s,x}$) reaction of HSA in PBS minus HSA in PBS supplemented with various concentrations of (*A*) arginine and (*B*) sucrose. Individual peptide fragments are listed on the *x* axis from the N- to the C-terminus. $\Delta D_{10s,x}$ values for each HSA peptide fragment were calculated as the deuterium uptake of the peptide fragment in the absence of excipient minus the deuterium uptake of the peptide fragment in the presence of excipient. Thus, positive values indicate that the excipient protects the peptide from deuteration, and negative values indicate that the excipient deprotects the peptide from deuteration. Representative peptides are shown as (*) and (#) and the difference in deuterium uptake as a function of excipient concentration is shown in (*C*) and (*D*). The correlation of the SILCS-Biologics metric, number of bound excipients (*y* axis) to HDX-MS-derived $\Delta D_{10s,100mM}$ for individual HSA peptide fragment (*x* axis) is shown for (*E*) arginine and (*F*) sucrose. The number of bound excipients per peptide fragment were calculated as the sum of occupancies of all compounds interacting with the given peptide. Each data point is colored based on the location of the corresponding peptide in the full-length HSA sequence, with blue corresponding to the N-terminus of HSA, and yellow corresponding to the C-terminus of HSA.

1000 s time point (negative $\Delta D_{1000s,100mM}$, supporting material, hdx-ms_duptake.xlsx). To understand this, we visually inspected the SILCS-Biologics predicted poses of arginine interacting with HSA. Notably, the predicted poses of arginine interacting with HSA represent their initial interaction before local unfolding events. Interestingly, regions containing HSA peptide fragments with positive $\Delta D_{10s,100mM}$ values and negative $\Delta D_{1000s,100mM}$ values involve arginine poses in proximity to salt bridges or cation-π interactions (Fig. 6). At these sites, arginine may disrupt stabilizing intramolecular interactions, thereby inducing local unfolding of HSA. Possible local unfolding may occur in peptides directly bound by arginine, or with peptides contiguous to those directly bound by arginine. Specifically, arginine appears to disrupt the intramolecular π-π interactions formed by Phe27, Tyr30, Phe70, and Phe102 at DS 10 (Fig. 6 *D*), leading to negative $\Delta D_{100s,100mM}$ and $\Delta D_{1000s,100mM}$ for peptides encompassing those residues in addition to peptides representing the HSA N-terminus (residues 1–25), and intramolecular cation-π interactions formed by Arg144 and Tyr140, and Lys137 and Phe36, π-π interactions formed by Phe36 and Tyr140, and salt bridges formed by Arg145 and Glu141, and Lys137 and Glu37 at ES 3 (Fig. 6 *B*).

Please cite this article in press as: Orr et al., Mapping the distribution and affinities of ligand interaction sites on human serum albumin, Biophysical Journal (2025), https://doi.org/10.1016/j.bpj.2025.03.016

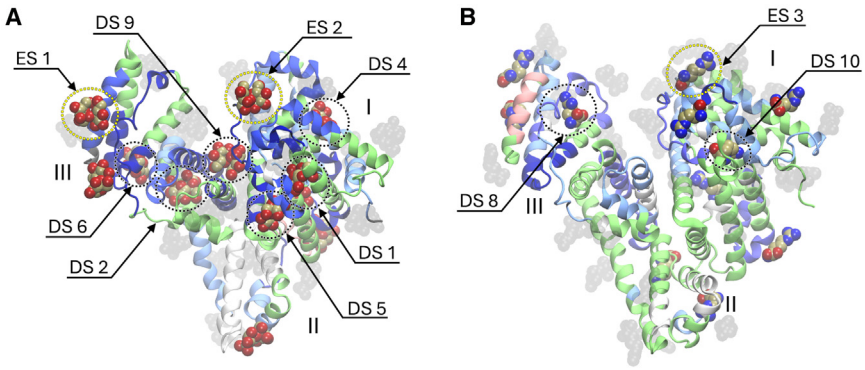

FIGURE 5 Interaction sites of (*A*) sucrose and (*B*) arginine to HSA predicted by SILCS-Biologics and observed with HDX-MS experiments at t = 10 s. Sucrose and arginine compounds are shown in van der Waals representation. Sucrose and arginine poses with occupancies predicted to be less than 0.9 by SILCS-Biologics are shown in transparent gray. HSA is shown in cartoon representation and is colored based on HDX-MS-derived $\Delta D_{10s,100mM}$, with dark blue representing $\Delta D_{10s,100mM} > 1$, blue representing $1 > \Delta D_{10s,100mM} > 0.5$, light blue representing $0.5 > \Delta D_{10s,100mM} > 0.25$, green representing $0.25 > \Delta D_{10s,100mM} > -0.25$, light red representing $-0.25 > \Delta D_{10s,100mM} > -0.5$, white representing residues not represented in the HDX-MS data, and gray representing flexible N- and C-termini.

Additionally, at DS 8, arginine may disrupt the intramolecular π-π network formed by Phe502, 507, 509, 551, 554, and 568 as well as the intramolecular salt bridges between Glu531 and Lys500 and Asp512 and Lys524 (Fig. 6 *C*). Thus, based on data extracted from SILCS-Biologics, arginine excipients favorably interact with HSA, resulting in positive $\Delta D_{10s,100mM}$ values, and over time the interactions of arginine with HSA residues involved in salt bridges, cation-π, or π-π interactions are hypothesized to disrupt these intramolecular interactions, resulting in potential local unfolding and negative $\Delta D_{1000s,100mM}$ values.

In the previous section, it was shown that HDX-MS experiments are able to reproduce previously determined binding affinities of ibuprofen and ketoprofen at known DSs on HSA including sites identified via crystallography. Binding affinities based on LGFEs from SILCS-Biologics were in satisfactory agreement with the experimental values, with the computational approach identifying additional binding sites and the associated LGFE values that were not accessible to K_d determination via HDX-MS, although the protection patterns do validate those sites as interacting with ibuprofen and ketoprofen. Building on this, affinities were measured using HDX for a subset of the interaction sites of sucrose and arginine that represent known DSs and newly identified excipient sites. The utility of HDX-MS in probing the effect of excipient and additives on protein and protein therapeutics has been previously demonstrated (36–42). However, to our knowledge, quantitative treatment to derive local binding affinity of excipient and additive with mM binding affinity has not previously been performed with HDX-MS. Here, we demonstrated HDX-MS versatility in providing localized binding affinities of excipients to proteins. Fig. 4, *C* and *D* display the $\Delta D_{10s,x}$ versus excipient concentration

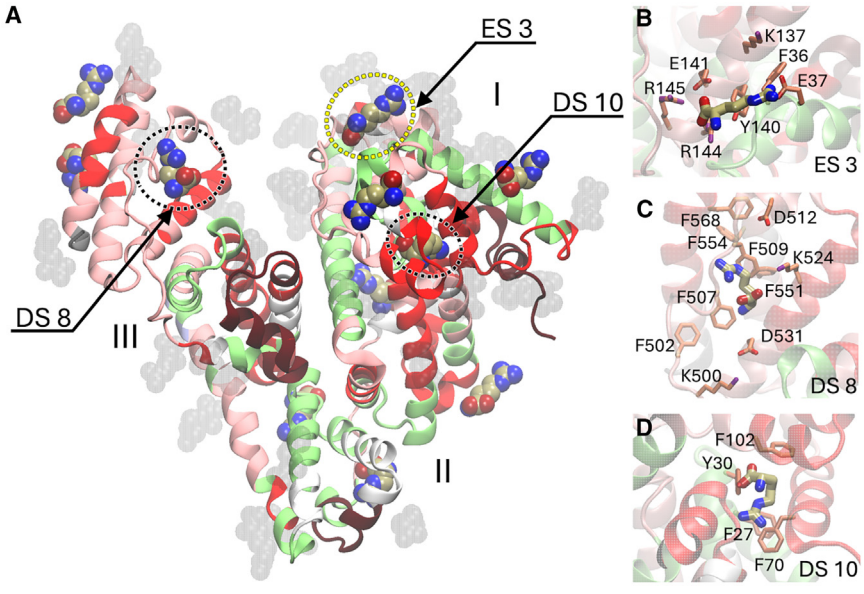

FIGURE 6 Interaction sites of arginine to HSA predicted by SILCS-Biologics and deprotection patterns observed for HSA in the presence of arginine at t = 1000 s by HDX-MS and (*B–D*) associated disrupted intramolecular interactions. (*A*) Arginine molecules are shown in van der Waals representation. arginine poses with occupancies predicted to be less than 0.9 by SILCS-Biologics are shown in transparent gray. HSA is shown in cartoon representation and is colored based on HDX-MS-derived $\Delta D_{1000s,100mM}$, with dark red representing $\Delta D_{1000s,100mM} < -1$, red representing $-1 < \Delta D_{1000s,100mM} < -0.5$, light red representing $-0.5 < \Delta D_{1000s,100mM} < -0.25$, green representing $-0.25 < \Delta D_{1000s,100mM} < 0.25$, and white representing residues not represented in the HDX-MS data, and gray representing flexible N- and C-termini. (*B–D*) HSA residues involved in intramolecular interactions and potentially disrupted by the presence of arginine are shown in licorice representation and arginine poses are shown in thick licorice representation.

Please cite this article in press as: Orr et al., Mapping the distribution and affinities of ligand interaction sites on human serum albumin, Biophysical Journal (2025), https://doi.org/10.1016/j.bpj.2025.03.016

TABLE 2 Affinities of sucrose and arginine to HSA and individual HSA peptide fragments derived by SILCS-Biologics (LGFE) and HDX-MS (K_d and ΔG) and their association to HSA drug sites

Drug site	LGFE (kcal/mol)	Peptide fragment sequence	HSA residue range	K_d (mM)	ΔG (kcal/mol)
Sucrose					
DS 1	−8.98	ASLQKFGERAFKAWAVARL	201–219	8.44 ± 3.54	−2.83
DS 2	−7.55	AKVFDEFKPLVEEPQNL	371–387	11.10 ± 8.03	−2.67
		VEVSRNLGKVGSKCCKHPEAKRMPCAE	424–450	7.76 ± 4.44	−2.88
		VEVSRNLGKVGSKCCKHPEAKRMPCAED	424–451	8.63 ± 4.61	−2.81
DS 4	−6.07	HDNEETF	128–134	8.36 ± 4.14	−2.83
DS 5	−4.47	VTDLTKVHTECCHGDL	235–250	16.11 ± 9.97	−2.44
		VTDLTKVHTECCHGDLLE	235–252	15.89 ± 6.18	−2.45
DS 6	−5.98	VELVKHKPKATKEQLKA	530–546	4.30 ± 2.51	−3.23
		VELVKHKPKATKEQLKAVMDD	530–550	6.79 ± 4.05	−2.96
		LVKHKPKATKEQLKAVM	532–548	6.09 ± 2.49	−3.02
DS 9	−5.25	VEVSRNLGKVGSKCCKHPEAKRMPCAE	424–450	7.76 ± 4.44	−2.88
		VEVSRNLGKVGSKCCKHPEAKRMPCAED	424–451	8.63 ± 4.61	−2.81
ES 1	−2.95	FAQYLQQCPFEDHVKLVNE	27–45	5.14 ± 1.19	−3.12
		LQQCPFEDHVKL	31–42	3.25 ± 1.48	−3.39
		LQQCPFEDHVKLVNE	31–45	5.00 ± 1.97	−3.14
ES 2	−4.67	*TYVPKEFNAET	*496–506	*3.76 ± 4.39	−3.31
		FTFHADICTLSEKERQIKKQTAL	507–529	3.72 ± 2.23	−3.31
Arginine					
DS 8	−3.59	EVDETYVPKEFNAET	492–506	4.90 ± 6.33	−3.15
		FTFHADICTLSEKERQIKKQTAL	507–529	8.13 ± 13.07	−2.85
		VELVKHKPKATKEQLKAVMDD	530–550	5.33 ± 6.36	−3.10
DS 10	−2.91	LQHKDDNPNLPRLVRPEVD	103–121	6.69 ± 5.95	−2.96
		LQHKDDNPNLPRLVRPEVDVM	103–123	5.38 ± 5.63	−3.09
		*VTDLTKVHTECCHGDL	*235-250	*0.32 ± 0.47	*-4.76
ES 3	−3.31	LQHKDDNPNLPRLVRPEVD	103–121	6.69 ± 5.95	−2.96
		LQHKDDNPNLPRLVRPEVDVM	103–123	5.38 ± 5.63	−3.09
		PRLVRPEVD	113–121	13.31 ± 15.80	−2.56

Peptide fragments deprotected by the presence of the excipients are denoted by *; all other peptide fragments were protected from deuteration. Peptide fragments may be associated with multiple drug sites.

of representative peptides for arginine and sucrose, respectively. The resulting curve is fit to a single site binding isotherm to derive a dissociation constant, K_d (Table 2; supporting material, HDX_Ligand_Titrations_Figures.pptx).

The HDX-MS-derived affinities of sucrose and arginine to individual HSA peptide fragments in proximity to the drug or excipient sites along with the LGFEs from SILCS-Biologics are listed in Table 2. Overall, the HDX-MS and SILCS-Biologics binding free energies are in reasonable agreement, being within ∼2–3 kcal/mol. However, large discrepancies occur with sucrose poses at DSs 1 and 2 where the SILCS-Biologics-derived LGFEs are much more favorable than the experimental values. Analysis of these sites (Fig. 5 *A*) along with calculation of their %rBSA values show them to be highly buried sites (%rBSA >70%, supporting material, silcs-biologics_poses.xlsx). The calculated LGFEs of sucrose are largely based on the SILCS methanol FragMaps associated with the hydroxyl oxygens of sucrose falling in that atom classification (Fig. S1). As sucrose is more hydrophilic than methanol, with a logP of −3.30 compared with methanol's logP of −0.77 (105,106), this may lead to the LGFEs for the buried poses of sucrose not sufficiently accounting for its unfavorable desolvation energy upon going from the water environment into the buried environment in the protein, thereby leading to an overestimation of the energetic favorability of buried poses of sucrose.

Overall correlation of SILCS-Biologics and HDX-MS binding affinities

Further analysis combining the ibuprofen, ketoprofen, sucrose, and arginine binding affinity data was performed to check the trends across the different chemical species. The HDX-MS-derived affinities are plotted versus the SILCS-Biologics LGFE values in Fig. 7. Note that, as several peptide fragments encompass similar sequence ranges, only the peptides displaying the most favorable affinities were retained per overlapping sequence range for the correlation analysis. As discussed above, both SILCS-Biologics and HDX-MS reproduce previously measured binding affinities of ibuprofen and ketoprofen (Fig. 7) (93–96). With respect to all other interactions of all four compounds for which HDX-MS K_d values were obtained, reasonable correlations were obtained with respect to K_d values from both

Please cite this article in press as: Orr et al., Mapping the distribution and affinities of ligand interaction sites on human serum albumin, Biophysical Journal (2025), https://doi.org/10.1016/j.bpj.2025.03.016

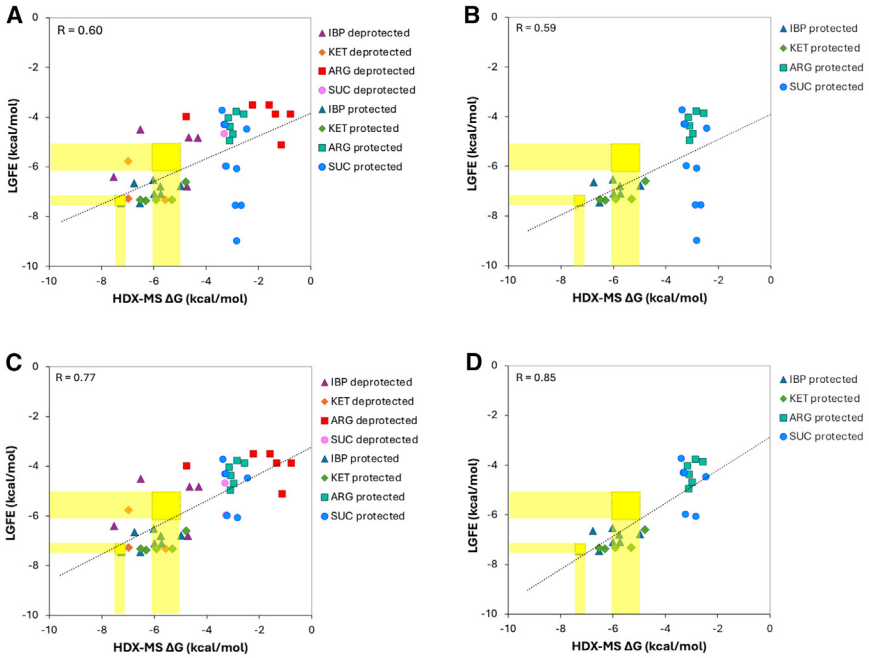

FIGURE 7 Correlation of SILCS-Biologics-derived LGFEs (*y* axis) with HDX-MS-derived ΔG (*x* axis) for ibuprofen (*triangles*), ketoprofen (*diamonds*), arginine (*squares*), and sucrose (*circles*). Results are shown for (*A*) all peptides for which K_d values were derived, (*B*) only protected peptides for which K_d values were derived, (*C*) all peptides for which K_d values were derived with the three outlier sucrose data points omitted, and (*D*) only protected peptides for which K_d values were derived with three outlier sucrose data points omitted. Regions highlighted in yellow correspond to the affinities of ibuprofen (ranging from −7.16 to −7.55 kcal/mol) and ketoprofen (ranging from −5.08 to −6.17 kcal/mol) reported in previous studies (93–96).

protection and deprotection (Fig. 7 *A*) as well as when only protection-based K_d values were used (Fig. 7 *B*). However, three data points for sucrose that have LGFE values significantly more favorable than the HDX-MS-derived affinities are evident. These sites are associated with DS 1 and DS 2 discussed above. As these sites are highly buried, we believe that the LGFEs of sucrose at these sites do not sufficiently account for unfavorable desolvation energy upon binding due to the use of SILCS methanol FragMaps to describe sucrose hydroxyl oxygens, resulting in an overestimated predicted affinity. Once these data points are omitted, the alignment between SILCS-Biologics LGFEs and HDX-MS-derived affinities is obvious, with significantly improved correlation and low RMSE (R = 0.77, RMSE = 1.76) when all the HDX-MS values are considered. Omission of affinities derived from deprotected HSA peptide fragments show an even higher correlation and lower RMSE (R = 0.85, RMSE = 1.73; Fig. 7 *D*).

The improvement in the agreement between LGFE values and HDX-MS-derived binding affinities when affinities derived from deprotected HSA peptide fragments are omitted may be attributed to a number of factors. If the deprotection of the peptide fragment is due to the binding of the compound to a separate peptide fragment leading to allosteric local conformational changes, as discussed for arginine at DS6, then the HDX-MS-derived affinity may reflect the compound's affinity to the separate peptide fragment rather than the deprotected fragment from which the LGFE value is determined. In addition, affinities derived for deprotected regions also include the effects and energetic contributions of local unfolding. Nonetheless, the SILCS-Biologics LGFEs are nicely correlated with HDX-MS-derived affinities as well as with previous experimental studies for ibuprofen and ketoprofen (Fig. 7) (93–96).

Another issue is the LGFE values typically being more favorable than the HDX-MS affinities for the excipients (Table 2; Fig. 7). In the experiments, the lowest concentration in titration was 0.1 mM for sucrose and arginine. Accordingly, as the HDX-MS method indirectly measures affinity by measuring changes in deuterium uptake in peptide fragments and that the lowest tested concentration is 0.1 mM, the lowest observable K_d for a given interaction is 0.1 mM. Assuming a K_d of 0.1 mM, the corresponding binding free energy would be approximately −5.45 kcal/mol. In particular, this may contribute to the discrepancy between the SILCS-Biologics and HDX-MS affinities observed at DS 1 and 2 with sucrose.

Stability studies

To gain insights into how the most favorable binding sites observed using SILCS-Biologics and HDX-MS impact protein stability we measured HSA stability through temperature ramp experiments on sucrose and arginine and additionally with alanine and trehalose. As opposed to the HDX-MS experiments performed with a low HSA concentration (∼20 μM) in the presence of a high excess of excipients, the stability measurements were performed with a millimolar HSA concentration and a maximum excipient/protein ratio of 265. In general, at low excipient/HSA ratios (ratios less than 66), the investigated excipients increase or minimally change ΔTm t_0 and ΔPreTm t_0 (Table 3), indicating that the excipients generally stabilize or at minimum

Please cite this article in press as: Orr et al., Mapping the distribution and affinities of ligand interaction sites on human serum albumin, Biophysical Journal (2025), https://doi.org/10.1016/j.bpj.2025.03.016

TABLE 3 Change in HSA melting temperatures at time t_0 (ΔPreTm t_0 and ΔTm t_0) of HSA in the presence of arginine (Arg), sucrose (Suc), alanine (Ala), and trehalose (Tre)

			ΔPreTm t_0 (°C)				ΔTm t_0 (°C)			
Excipient/HSA ratio	[HSA]	[Excipient]	Arg	Suc	Ala	Tre	Arg	Suc	Ala	Tre
16	7.54	125	−5.38	3.68	−1.00	7.99	5.33	3.99	−0.64	6.01
33	7.54	250	4.67	5.98	6.35	9.66	6.98	4.99	4.67	6.66
33	3.77	125	−1.66	5.01	1.34	7.68	5.68	4.33	0.03	6.68
66	7.54	500	3.32	6.01	9.99	7.68	2.32	5.99	7.00	5.97
66	3.77	250	6.32	6.69	6.35	9.66	7.02	5.66	4.02	7.04
66	1.88	125	−3.02	6.30	−2.33	3.65	−0.34	0.28	−0.35	−3.67
132	3.77	500	7.33	4.87	9.99	7.68	7.02	7.01	8.02	6.99
132	1.88	250	−1.34	8.98	1.98	2.34	−4.67	0.31	−5.02	−4.03
265	1.88	500	1.99	10.99	1.97	1.98	−5.01	0.98	−6.01	−1.01

The concentrations of HSA and the excipients are listed in mM. For HSA, 7.54 mM corresponds to 500 mg/mL, 3.77 mM to 250 mg/mL, and 1.88 mM to 125 mg/mL.

do not destabilize HSA. At higher excipient/HSA ratios, sucrose still consistently increases the ΔTm t_0 and ΔPreTm t_0 of HSA (Table 3) while arginine generally decreases ΔTm t_0 and ΔPreTm t_0 (Table 3). These results are generally consistent with HDX-MS experiments showing that sucrose protects HSA from deuteration at all time periods, whereas arginine progressively deprotects HSA from deuteration at longer times (Figs. 6 and S2; supporting material, hdx-ms_duptake.xlsx) associated with the nature of the interactions of arginine with HSA as predicted by SILCS (Fig. 6). Additionally, the stabilization of HSA by sucrose observed across different excipients/HSA ratios is in line with previous studies showing that sucrose protects HSA from thermal and chemical denaturation (103,104). The ΔTm t_0 of HSA in the presence of alanine shows a similar trend to arginine, with higher excipient/HSA ratios leading to destabilization (Table 3). Overall, the trends in ΔTm and ΔPreTm observed at t_0 are also observed in t_1, with higher rates of destabilization (decreased ΔTm t_1 and ΔPreTm t_1) observed for higher excipient/HSA ratios (Table 4).

Quantitative SILCS-Biologics metrics were examined to identify potential indicators that may be used to predict the effect of excipients on HSA. Metrics calculated from SILCS-Biologics for the four excipients were subjected to correlation analysis against the ΔTm and ΔPreTm data at the different excipient concentrations and different time points. At low excipient/HSA ratios, ΔTm t_0 values correlate well with the SILCS-Biologics metric sum of interaction site occupancies involved in PPI based on SILCS PPIP values greater than 0.2 (Fig. 8 *A*). As SILCS-Biologics occupancies are calculated using excipient concentrations without including the protein concentration, the correlation analysis was performed with occupancies calculated using high (500 mM) and low (5 mM) concentrations of excipients. Nonetheless, using both high and low concentrations of excipients as input resulted in high correlations ($R > 0.8$) with ΔTm t_0 values for the lowest excipient/HSA ratio (Fig. 8 *A*). At high excipient/HSA ratios, ΔTm t_0 values correlate well with the SILCS-Biologics metrics associated with the energetic favorability of the excipients interacting with HSA (Fig. 8 *B*) as well as the sum of interaction site occupancies of sites near HSA intramolecular interactions using occupancy values calculated using both high and low excipient concentrations (Fig. 8 *C*). The correlation of the sum of interaction site occupancies with PPIP values greater than 0.2 with ΔTm t_0 suggests that the ability of excipients to bind to HSA regions participating in PPI that may contribute to aggregation becomes

TABLE 4 Change in HSA melting temperatures at time t_1 (ΔPreTm t_1 and ΔTm t_1) of HSA in the presence of arginine (Arg), sucrose (Suc), alanine (Ala), and trehalose (Tre)

			ΔPreTm t_1 (°C)				ΔTm t_1 (°C)			
Excipient:HSA ratio	[HSA]	[Excipient]	Arg	Suc	Ala	Tre	Arg	Suc	Ala	Tre
16	7.54	125	−0.03	0.98	0.33	2.31	0.7	0.66	0.33	0.34
33	7.54	250	0.26	1.96	−1.36	3.00	0.36	0.33	−1.67	0.68
33	3.77	125	5.62	3.67	−0.37	1.99	0.3	1.36	0.01	0.02
66	7.54	500	2.99	2.66	4.00	−1.33	0.66	1.02	1.00	0.71
66	3.77	250	6.01	1.33	−1.68	1.98	0.69	0.66	−0.99	1.67
66	1.88	125	−2.33	−0.66	−3.68	−3.32	−2.97	−2.67	1.35	−1.68
132	3.77	500	2.33	0.03	1.67	2.99	0.66	0.34	0.67	0.97
132	1.88	250	−2.67	−5.64	3.66	−5.65	−3.01	−3.68	3.65	−2.33
265	1.88	500	−2.99	−2.00	−5.34	−3.33	−3.67	−2.02	−1.98	−1.66

The concentrations of HSA and the excipients are listed in mM. For HSA, 7.54 mM corresponds to 500 mg/mL, 3.77 mM to 250 mg/mL, and 1.88 mM to 125 mg/mL.

Please cite this article in press as: Orr et al., Mapping the distribution and affinities of ligand interaction sites on human serum albumin, Biophysical Journal (2025), https://doi.org/10.1016/j.bpj.2025.03.016

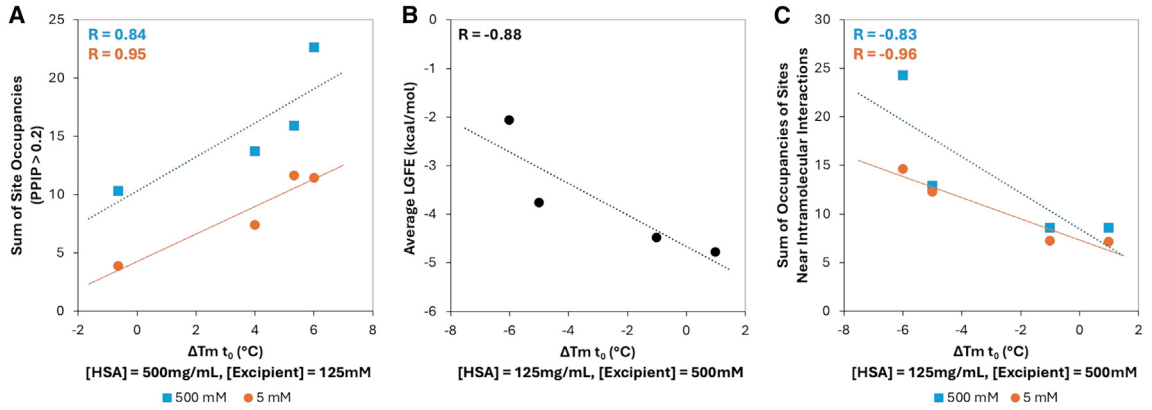

FIGURE 8 Correlation of SILCS-Biologics metrics with ΔTm at t_0 for (*A*) the excipient/HSA ratio of 16 ([HSA] = 7.54 mM (500 mg/mL) and [excipient] = 125 mM) and (*B* and *C*) the excipient/HSA ratio of 265 ([HSA] = 1.88 mM (125 mg/mL) and [excipient] = 500 mM). (*A* and *C*) SILCS-Biologics occupancy values were calculated using an excipient concentration of 500 mM (*blue*, *square data points*) and 5 mM (*orange*, *circle data points*). Results are presented for (*A*) the sum of the site occupancies for sites with PPIP > 0.2, (*B*) the average LGFE of all excipient poses, and (*C*) the sum of the site occupancies for sites near HSA intramolecular interactions.

increasingly important and that PPI is a key driving force behind HSA stability at high HSA concentrations. Conversely, at low concentrations of HSA, PPI and the ability of excipients to block regions of high PPIP is negligible as the probability of HSA PPI decreases as the HSA concentration decreases. This is evident as the correlation of the sum of interaction site occupancies with PPIP values greater than 0.2 with the ΔTm t_0 values decreases to $R < 0.25$ (not shown). At low concentrations, simply the average LGFE, representing the energetic favorability of excipients interacting with HSA, can indicate favorable excipients (Fig. 8 *B*). At low HSA concentrations, the interaction of the excipients with the folded state of the protein may increase its stability. Additionally, excipients with more interaction sites in proximity to intramolecular HSA interactions, thereby potentially disrupting the intramolecular interactions, are correlated with less protective or deprotective behavior observed in the stability studies at high excipient/HSA ratios (Fig. 8 *C*), with both arginine and alanine interacting with the most sites near stabilizing intramolecular HSA interactions. These results emphasize consideration of the concentrations of the excipients and of the protein when using SILCS-Biologics metrics to predict the impact of excipients on protein stability.

DISCUSSION

Weak and transient small-molecule interactions with proteins play crucial roles in biological processes, including signal regulation, metabolism, and allosteric regulation. In the context of drug discovery and biologics formulations, low-affinity molecules are especially valuable. In drug discovery, low-affinity small molecules serve as initial building blocks in fragment-based approaches, where initial weak binders are optimized to enhance potency and selectivity while minimizing off-target effects (1–6). In biologics formulations, excipients, which often exhibit low-affinity binding characteristics, are critical for stabilizing protein therapeutics, improving their solubility and stability by binding to the active, folded state of the protein and by preventing protein aggregation (7–10). Despite the importance of low-affinity interactions in both biological processes and in the development of therapeutics, mapping such interactions poses challenges due to their transient nature, which eludes conventional structural biology techniques such as x-ray crystallography and NMR. In this study, we use a combined approach of SILCS-Biologics, HDX-MS, and accelerated stability studies to elucidate the interactions of both high-affinity ligands as well as low-affinity excipients and determine how low-affinity interactions by excipients affect protein stability in the context of protein therapeutic formulation.

Our investigation of known HSA ligands ibuprofen and ketoprofen demonstrate that SILCS-Biologics effectively predicted binding sites for both compounds, including sites that were consistent with those observed in previous crystallography studies (91,92). The integration of HDX-MS data with SILCS-Biologics allowed the identification of additional potential interaction sites of ibuprofen and ketoprofen that were unresolved in crystal structures, supporting previous hypotheses of and experiments suggesting multiple binding sites for these ligands beyond those that were crystal resolved within serum albumins (96–102). At 750 μM over 20 interaction sites for each compound were identified. Several factors may contribute to the sites identified in this study being unresolved in previously constructed crystal structures. In the structure of ketoprofen bound to HSA, DSs 6 and 8, which were shown in this study to be ketoprofen binding sites, are occupied by mysteric acid, which was not included in our studies (91). Additionally, the use of high concentrations of DMSO in both the crystal structures of ketoprofen and ibuprofen binding to HSA may affect the

folding of HSA as observed for other serum albumins (107) or lower the affinity of the ligands by altering the dielectric environment of the solvent and creating competition between the DMSO solvent and protein environment upon binding (108,109). Furthermore, crystal contacts may also influence the binding and resolution of the compounds in the crystal structures. In the structure of ibuprofen bound to HSA, DSs 6 and 8 could be obstructed by neighboring HSA monomers within the crystal lattice (Fig. S3) (92). Both HDX-MS-derived affinities and SILCS-Biologics LGFEs, representing the ligand binding free energy, show that the ligands bind HSA with micromolar affinity, in line with previously determined affinities derived through conventional experimental methods (93–96). Beyond the identified high affinity poses of ibuprofen and ketoprofen, low-affinity interactions were detected throughout the HSA structure by both SILCS-Biologics and HDX-MS. Correlation analysis showed fair agreement between the HDX-MS-derived protection/deprotection patterns and SILCS-Biologics predicted interactions, strengthening the validity of the predictive power of SILCS-Biologics for studying low-affinity interactions that are otherwise difficult to capture through traditional structural techniques.

The application of SILCS-Biologics and HDX-MS on excipients, sucrose and arginine, exhibited distinct interaction behaviors. Sucrose, which consistently protected HSA against deuteration, was found to occupy both drug and excipient sites at the interior of HSA in addition to interaction sites at the surface of HSA. Conversely, arginine was found to bind to over 40 sites but have less favorable binding affinities than sucrose, which occupied more than 20 sites, with the majority of arginine interaction sites occurring at the surface of HSA. Additionally, while sucrose protected HSA from deuteration at both short and long timescales, prolonged exposure to arginine of HSA led to local unfolding as indicated by negative $\Delta D_{1000s,x}$ values from HDX-MS. The SILCS-Biologics simulations suggest that arginine's disruptive effect is due to its interaction with stabilizing intramolecular salt bridge, π-π, and cation-π interactions, ultimately leading to local unfolding of HSA at longer timescales. Accelerated stability studies of HSA in the presence of excipients sucrose, arginine, trehalose, and alanine show that at low excipient/HSA ratios, the excipients generally stabilize HSA. At high excipient/HSA ratios, sucrose still has a stabilizing effect on HSA, in line with previous studies that highlight sucrose's protective effect against protein denaturation (103,104), whereas arginine destabilizes HSA. Combining the insights gained from SILCS-Biologics, HDX-MS, and accelerated stability studies, the destabilization of HSA by arginine may be attributed to the disruption of important intramolecular interactions, leading to local unfolding, and ultimately leading to a less stable HSA formulation.

The quantitative agreement between SILCS-Biologics-derived LGFEs and HDX-MS-derived binding affinities further highlights the utility of the SILCS-Biologics approach. With the exception of three SILCS-Biologics predicted poses of sucrose, LGFEs and HDX-MS-derived affinities were in strong agreement, with an R of 0.77 and RMSE of 1.73 kcal/mol when considering only affinities derived from protected peptide fragments. The strong correlation for both high-affinity and low-affinity ligands demonstrates that SILCS-Biologics is capable of capturing the energetics of weak interactions as previously observed in a study of multiple excipients interacting with a monoclonal antibody (66). Such estimations are critical in the context of biologics formulations, as correlation analysis between SILCS-Biologics metrics and melting temperatures derived from accelerated stability studies showed that metrics involving excipient occupancies, calculated as a function of LGFE and excipient concentration, along with consideration of sites involved in PPI, achieve the most predictive power.

Overall, our study demonstrates the synergistic potential of combining SILCS-Biologics with HDX-MS and accelerated stability studies for mapping complex protein-ligand/excipient interactions that can inform and predict excipient effects on formulation stability. By providing atomic-level insights into interaction sites and affinities, this combined approach can describe transient, low-affinity interactions to guide the rational design of excipients for biologics formulation, enabling optimization of protein stability. Future work could expand on this approach by applying it to other biologically relevant proteins and excipients to further enhance formulation strategies.

ACKNOWLEDGMENTS

The authors acknowledge financial support from NIH R35GM131710 and R44GM130198. All computational analyses were performed with computational resources provided by the Computer-Aided Drug Design (CADD) Center at the University of Maryland, Baltimore and SilcsBio LLC.

AUTHOR CONTRIBUTIONS

S.W.H., D.J.D., and A.D.M. conceived the study and designed the experiments. A.A.O., A.U., X.L., and A.K.K. performed the experiments and collected the data. A.A.O., A.U., X.L., A.K.K., S.W.H., D.D., and A.D.M. analyzed the data and interpreted the results. D.E. contributed to the theoretical framework and provided critical feedback. A.A.O., S.W.H., D.J.D., and A.D.M. wrote the manuscript with input from all authors. A.D.M., S.W.H., and D.J.D. supervised the project and provided funding. All authors have read and approved the final manuscript.

DECLARATION OF INTERESTS

A.D.M. is cofounder and CSO of SilcsBio LLC.

SUPPORTING MATERIAL

Supporting material can be found online at https://doi.org/10.1016/j.bpj.2025.03.016.

Please cite this article in press as: Orr et al., Mapping the distribution and affinities of ligand interaction sites on human serum albumin, Biophysical Journal (2025), https://doi.org/10.1016/j.bpj.2025.03.016

REFERENCES

1. Hartshorn, M. J., C. W. Murray, …, H. Jhoti. 2005. Fragment-Based Lead Discovery Using X-ray Crystallography. *J. Med. Chem.* 48:403–413.
2. Harner, M. J., A. O. Frank, and S. W. Fesik. 2013. Fragment-based drug discovery using NMR spectroscopy. *J. Biomol. NMR.* 56:65–75.
3. Bollag, G., J. Tsai, …, P. Hirth. 2012. Vemurafenib: the first drug approved for BRAF-mutant cancer. *Nat. Rev. Drug Discov.* 11:873–886.
4. Bollag, G., P. Hirth, …, K. Nolop. 2010. Clinical efficacy of a RAF inhibitor needs broad target blockade in BRAF-mutant melanoma. *Nature.* 467:596–599.
5. Doak, B. C., R. S. Norton, and M. J. Scanlon. 2016. The ways and means of fragment-based drug design. *Pharmacol. Ther.* 167:28–37.
6. Murray, C. W., and D. C. Rees. 2009. The rise of fragment-based drug discovery. *Nat. Chem.* 1:187–192.
7. Roberts, C. J. 2014. Therapeutic protein aggregation: mechanisms, design, and control. *Trends Biotechnol.* 32:372–380.
8. Kamerzell, T. J., R. Esfandiary, …, D. B. Volkin. 2011. Protein–excipient interactions: Mechanisms and biophysical characterization applied to protein formulation development. *Adv. Drug Deliv. Rev.* 63:1118–1159.
9. Wang, W. 1999. Instability, stabilization, and formulation of liquid protein pharmaceuticals. *Int. J. Pharm.* 185:129–188.
10. Ohtake, S., Y. Kita, and T. Arakawa. 2011. Interactions of formulation excipients with proteins in solution and in the dried state. *Adv. Drug Deliv. Rev.* 63:1053–1073.
11. Orts, J., and A. D. Gossert. 2018. Structure determination of protein-ligand complexes by NMR in solution. *Methods.* 138–139:3–25.
12. Ardenkjaer-Larsen, J., G. S. Boebinger, …, L. Frydman. 2015. Facing and Overcoming Sensitivity Challenges in Biomolecular NMR Spectroscopy. *Angew. Chem. Int. Ed.* 54:9162–9185.
13. Acharya, K. R., and M. D. Lloyd. 2005. The advantages and limitations of protein crystal structures. *Trends Pharmacol. Sci.* 26:10–14.
14. Benjin, X., and L. Ling. 2020. Developments, applications, and prospects of cryo-electron microscopy. *Protein Sci.* 29:872–882.
15. Malde, A. K., and A. E. Mark. 2011. Challenges in the determination of the binding modes of non-standard ligands in X-ray crystal complexes. *J. Comput. Aided Mol. Des.* 25:1–12.
16. Jankovics, H., B. Kovacs, …, R. Horvath. 2020. Grating-coupled interferometry reveals binding kinetics and affinities of Ni ions to genetically engineered protein layers. *Sci. Rep.* 10:22253.
17. Jug, A., T. Bratkovič, and J. Ilaš. 2024. Biolayer interferometry and its applications in drug discovery and development. *TrAC, Trends Anal. Chem.* 176:117741.
18. Oshannessy, D. J., M. Brighamburke, …, I. Brooks. 1993. Determination of Rate and Equilibrium Binding Constants for Macromolecular Interactions Using Surface Plasmon Resonance: Use of Nonlinear Least Squares Analysis Methods. *Anal. Biochem.* 212:457–468.
19. Menéndez, M. 2020. Isothermal Titration Calorimetry: Principles and Applications. *In* Encyclopedia of Life Sciences Wiley, pp. 113–127.
20. Saponaro, A. 2018. Isothermal Titration Calorimetry: A Biophysical Method to Characterize the Interaction between Label-free Biomolecules in Solution. *Bio. Protoc.* 8:e2957.
21. Kochert, B. A., R. E. Iacob, …, J. R. Engen. 2018. Hydrogen-Deuterium Exchange Mass Spectrometry to Study Protein Complexes. *Methods Mol. Biol.* 1764:153–171.
22. Jaswal, S. S. 2013. Biological insights from hydrogen exchange mass spectrometry. *Biochim. Biophys. Acta.* 1834:1188–1201.
23. Gallagher, E. S., and J. W. Hudgens. 2016. Mapping Protein–Ligand Interactions with Proteolytic Fragmentation, Hydrogen/Deuterium Exchange-Mass Spectrometry. *Methods Enzymol.* 566:357–404.
24. James, E. I., T. A. Murphree, …, M. Guttman. 2022. Advances in Hydrogen/Deuterium Exchange Mass Spectrometry and the Pursuit of Challenging Biological Systems. *Chem. Rev.* 122:7562–7623.
25. Majumdar, R., C. R. Middaugh, …, D. B. Volkin. 2015. Hydrogen-Deuterium Exchange Mass Spectrometry as an Emerging Analytical Tool for Stabilization and Formulation Development of Therapeutic Monoclonal Antibodies. *J. Pharmaceut. Sci.* 104:327–345.
26. Zhang, Z., and D. L. Smith. 1993. Determination of amide hydrogen exchange by mass spectrometry: A new tool for protein structure elucidation. *Protein Sci.* 2:522–531.
27. Deredge, D., J. Li, …, P. L. Wintrode. 2016. Hydrogen/Deuterium Exchange Kinetics Demonstrate Long Range Allosteric Effects of Thumb Site 2 Inhibitors of Hepatitis C Viral RNA-dependent RNA Polymerase. *J. Biol. Chem.* 291:10078–10088.
28. Klontz, E. H., A. D. Tomich, …, E. J. Sundberg. 2017. Structure and Dynamics of FosA-Mediated Fosfomycin Resistance in Klebsiella pneumoniae and Escherichia coli. *Antimicrob. Agents Chemother.* 61:e01572-17.
29. Tomich, A. D., E. H. Klontz, …, N. Sluis-Cremer. 2019. Small-Molecule Inhibitor of FosA Expands Fosfomycin Activity to Multidrug-Resistant Gram-Negative Pathogens. *Antimicrob. Agents Chemother.* 63:e01524-18.
30. Centola, G., D. J. Deredge, …, A. Wilks. 2020. Gallium(III)–Salophen as a Dual Inhibitor of *Pseudomonas aeruginosa* Heme Sensing and Iron Acquisition. *ACS Infect. Dis.* 6:2073–2085.
31. Osterberg, M. K., A. K. Smith, …, D. P. Giedroc. 2024. Coupling of zinc and GTP binding drives G-domain folding in Acinetobacter baumannii ZigA. *Biophys. J.* 123:979–991.
32. Kihn, K. C., O. Purdy, …, D. J. Deredge. 2024. Integration of Hydrogen–Deuterium Exchange Mass Spectrometry with Molecular Dynamics Simulations and Ensemble Reweighting Enables High Resolution Protein–Ligand Modeling. *J. Am. Soc. Mass Spectrom.* 35:2714–2728.
33. Zhu, M. M., D. L. Rempel, …, M. L. Gross. 2003. Quantification of Protein−Ligand Interactions by Mass Spectrometry, Titration, and H/D Exchange: PLIMSTEX. *J. Am. Chem. Soc.* 125:5252–5253.
34. Huang, R. Y.-C., D. L. Rempel, and M. L. Gross. 2011. HD Exchange and PLIMSTEX Determine the Affinities and Order of Binding of Ca^{2+} with Troponin C. *Biochemistry.* 50:5426–5435.
35. Wang, H., D. L. Rempel, …, M. L. Gross. 2017. Peptide-Level Interactions between Proteins and Small-Molecule Drug Candidates by Two Hydrogen−Deuterium Exchange MS-Based Methods: The Example of Apolipoprotein E3. *Anal. Chem.* 89:10687–10695.
36. Karunaratne, S. P., M. C. Jolliffe, …, D. D. Weis. 2023. Interaction between preservatives and a monoclonal antibody in support of multi-dose formulation development. *Int. J. Pharm.* 648:123600.
37. Hu, Y., R. T. Toth, …, D. D. Weis. 2020. Characterization of Excipient Effects on Reversible Self-Association, Backbone Flexibility, and Solution Properties of an IgG1 Monoclonal Antibody at High Concentrations: Part 2. *J. Pharmaceut. Sci.* 109:353–363.
38. Toth, R. T., S. E. Pace, …, D. B. Volkin. 2018. Evaluation of Hydrogen Exchange Mass Spectrometry as a Stability-Indicating Method for Formulation Excipient Screening for an IgG4 Monoclonal Antibody. *J. Pharmaceut. Sci.* 107:1009–1019.
39. Arora, J., S. B. Joshi, …, D. B. Volkin. 2017. Correlating the Effects of Antimicrobial Preservatives on Conformational Stability, Aggregation Propensity, and Backbone Flexibility of an IgG1 mAb. *J. Pharmaceut. Sci.* 106:1508–1518.
40. Arora, J., Y. Hu, …, D. D. Weis. 2016. Charge-mediated Fab-Fc interactions in an IgG1 antibody induce reversible self-association, cluster formation, and elevated viscosity. *mAbs.* 8:1561–1574.
41. Manikwar, P., R. Majumdar, …, D. B. Volkin. 2013. Correlating Excipient Effects on Conformational and Storage Stability of an IgG1 Monoclonal Antibody with Local Dynamics as Measured by Hydrogen/Deuterium-Exchange Mass Spectrometry. *J. Pharmaceut. Sci.* 102:2136–2151.

Please cite this article in press as: Orr et al., Mapping the distribution and affinities of ligand interaction sites on human serum albumin, Biophysical Journal (2025), https://doi.org/10.1016/j.bpj.2025.03.016

42. Majumdar, R., P. Manikwar, …, D. D. Weis. 2013. Effects of Salts from the Hofmeister Series on the Conformational Stability, Aggregation Propensity, and Local Flexibility of an IgG1 Monoclonal Antibody. *Biochemistry.* 52:3376–3389.
43. Chai, R., F. Li, …, L. Qiu. 2024. Unveiling preferred chemoattractants for rhizosphere PGPR colonization by molecular docking and molecular dynamics simulations. *Comput. Electron. Agric.* 225:109266.
44. Fan, S., J. Liu, …, G. Rudenko. 2024. Molecular mechanism of contactin 2 homophilic interaction. *Structure.* 32:1652–1666.e8.
45. Orr, A. A., J. Yang, …, P. Tamamis. 2020. Molecular Mechanism for Attractant Signaling to DHMA by E. coli Tsr. *Biophys. J.* 118:492–504.
46. Hirano, Y., N. Okimoto, …, M. Taiji. 2021. Molecular Dynamics Study of Conformational Changes of Tankyrase 2 Binding Subsites upon Ligand Binding. *ACS Omega.* 6:17609–17620.
47. Diakogiannaki, I., M. Papadourakis, …, A. Koutselos. 2024. Computational Investigation of BMAA and Its Carbamate Adducts as Potential GluR2 Modulators. *J. Chem. Inf. Model.* 64:5140–5150.
48. Kihn, K. C., T. Wilson, …, D. J. Deredge. 2021. Modeling the native ensemble of PhuS using enhanced sampling MD and HDX-ensemble reweighting. *Biophys. J.* 120:5141–5157.
49. Petruk, A. A., L. A. Defelipe, …, A. G. Turjanski. 2013. Molecular Dynamics Simulations Provide Atomistic Insight into Hydrogen Exchange Mass Spectrometry Experiments. *J. Chem. Theor. Comput.* 9:658–669.
50. Bradshaw, R. T., F. Marinelli, …, L. R. Forrest. 2020. Interpretation of HDX Data by Maximum-Entropy Reweighting of Simulated Structural Ensembles. *Biophys. J.* 118:1649–1664.
51. Heid, L. F., E. D. Agerschou, …, W. Hoyer. 2024. Sequence-based identification of amyloidogenic β-hairpins reveals a prostatic acid phosphatase fragment promoting semen amyloid formation. *Comput. Struct. Biotechnol. J.* 23:417–430.
52. Eswar, N., B. Webb, …, A. Sali. 2006. Comparative Protein Structure Modeling Using Modeller. *Curr. Protoc. Bioinform.* Chapter 5:Unit-5.6.
53. Ge, Y., V. Pande, …, K. L. Damm-Ganamet. 2024. Exploring the Application of SiteMap and Site Finder for Focused Cryptic Pocket Identification. *J. Phys. Chem. B.* 128:6233–6245.
54. Bowman, G. R., E. R. Bolin, …, S. Marqusee. 2015. Discovery of multiple hidden allosteric sites by combining Markov state models and experiments. *Proc. Natl. Acad. Sci. USA.* 112:2734–2739.
55. Schmidtke, P., A. Bidon-Chanal, …, X. Barril. 2011. MDpocket: open-source cavity detection and characterization on molecular dynamics trajectories. *Bioinformatics.* 27:3276–3285.
56. Le Guilloux, V., P. Schmidtke, and P. Tuffery. 2009. Fpocket: An open source platform for ligand pocket detection. *BMC Bioinf.* 10:168.
57. Guvench, O., and A. D. MacKerell. 2009. Computational Fragment-Based Binding Site Identification by Ligand Competitive Saturation. *PLoS Comput. Biol.* 5:e1000435.
58. Raman, E. P., W. Yu, …, A. D. MacKerell. 2013. Inclusion of Multiple Fragment Types in the Site Identification by Ligand Competitive Saturation (SILCS) Approach. *J. Chem. Inf. Model.* 53:3384–3398.
59. Zhao, M., W. Yu, and A. D. MacKerell. 2024. Enhancing SILCS-MC via GPU Acceleration and Ligand Conformational Optimization with Genetic and Parallel Tempering Algorithms. *J. Phys. Chem. B.* 128:7362–7375.
60. Ustach, V. D., S. K. Lakkaraju, …, A. D. MacKerell. 2019. Optimization and Evaluation of Site-Identification by Ligand Competitive Saturation (SILCS) as a Tool for Target-Based Ligand Optimization. *J. Chem. Inf. Model.* 59:3018–3035.
61. MacKerell, A. D., S. Jo, …, W. Yu. 2020. Identification and characterization of fragment binding sites for allosteric ligand design using the site identification by ligand competitive saturation hotspots approach (SILCS-Hotspots). *Biochim. Biophys. Acta Gen. Subj.* 1864:129519.
62. Nordquist, E. B., M. Zhao, …, A. D. MacKerell. 2024. Combined Physics- and Machine-Learning-Based Method to Identify Druggable Binding Sites Using SILCS-Hotspots. *J. Chem. Inf. Model.* 64:7743–7757.
63. Yu, W., S. Jo, …, A. D. MacKerell. 2019. Exploring protein-protein interactions using the site-identification by ligand competitive saturation methodology. *Proteins.* 87:289–301.
64. Jo, S., A. Xu, …, A. D. MacKerell. 2020. Computational Characterization of Antibody–Excipient Interactions for Rational Excipient Selection Using the Site Identification by Ligand Competitive Saturation-Biologics Approach. *Mol. Pharm.* 17:4323–4333.
65. Somani, S., S. Jo, …, S. V. Thakkar. 2021. Toward Biotherapeutics Formulation Composition Engineering using Site-Identification by Ligand Competitive Saturation (SILCS). *J. Pharmaceut. Sci.* 110:1103–1110.
66. Zhang, C., S. T. Gossert, …, A. Abraham. 2023. Ranking mAb–excipient interactions in biologics formulations by NMR spectroscopy and computational approaches. *mAbs.* 15:2212416.
67. Orr, A. A., A. Tao, …, A. D. MacKerell. 2023. Site Identification by Ligand Competitive Saturation-Biologics Approach for Structure-Based Protein Charge Prediction. *Mol. Pharm.* 20:2600–2611.
68. Li, X., A. A. Orr, S. W. Hoag…, 2024. Investigating the Interaction between Excipients and Monoclonal Antibodies PGT121 and N49P9.6-FR-LS: A Comprehensive Analysis. *Mol. Pharm.* https://doi.org/10.1021/acs.molpharmaceut.4c00973.
69. Bihari, S., J. Bannard-Smith, and R. Bellomo. 2020. Albumin as a drug: its biological effects beyond volume expansion. *Crit. Care Resusc.* 22:257–265.
70. Czub, M. P., K. B. Handing, …, W. Minor. 2020. Albumin-Based Transport of Nonsteroidal Anti-Inflammatory Drugs in Mammalian Blood Plasma. *J. Med. Chem.* 63:6847–6862.
71. SUDLOW, G., D. J. BIRKETT, and D. N. WADE. 1975. The Characterization of Two Specific Drug Binding Sites on Human Serum Albumin. *Mol. Pharmacol.* 11:824–832.
72. SUDLOW, G., D. J. BIRKETT, and D. N. WADE. 1976. Further Characterization of Specific Drug Binding Sites on Human Serum Albumin. *Mol. Pharmacol.* 12:1052–1061.
73. He, X. M., and D. C. Carter. 1992. Atomic structure and chemistry of human serum albumin. *Nature.* 358:209–215.
74. Zhu, L., F. Yang, …, M. Huang. 2008. A new drug binding subsite on human serum albumin and drug–drug interaction studied by X-ray crystallography. *J. Struct. Biol.* 162:40–49.
75. Petitpas, I., C. E. Petersen, …, S. Curry. 2003. Structural basis of albumin–thyroxine interactions and familial dysalbuminemic hyperthyroxinemia. *Proc. Natl. Acad. Sci. USA.* 100:6440–6445.
76. Petitpas, I., A. A. Bhattacharya, …, S. Curry. 2001. Crystal Structure Analysis of Warfarin Binding to Human Serum Albumin. *J. Biol. Chem.* 276:22804–22809.
77. Lejon, S., J. F. Cramer, and P. Nordberg. 2008. Structural basis for the binding of naproxen to human serum albumin in the presence of fatty acids and the GA module. *Acta Crystallogr., Sect. F: Struct. Biol. Cryst. Commun.* 64:64–69.
78. Hein, K. L., U. Kragh-Hansen, …, P. Nissen. 2010. Crystallographic analysis reveals a unique lidocaine binding site on human serum albumin. *J. Struct. Biol.* 171:353–360.
79. Bhattacharya, A. A., S. Curry, and N. P. Franks. 2000. Binding of the General Anesthetics Propofol and Halothane to Human Serum Albumin. *J. Biol. Chem.* 275:38731–38738.
80. Wang, Z. m., J. X. Ho, …, D. C. Carter. 2013. Structural studies of several clinically important oncology drugs in complex with human serum albumin. *Biochim. Biophys. Acta.* 1830:5356–5374.
81. Handing, K. B., I. G. Shabalin, …, W. Minor. 2016. Crystal structure of equine serum albumin in complex with cetirizine reveals a novel drug binding site. *Mol. Immunol.* 71:143–151.
82. Jiang, B., A. Jain, …, S. W. Hoag. 2019. Probing Thermal Stability of Proteins with Temperature Scanning Viscometer. *Mol. Pharm.* 16:3687–3693.

83. Klontz, E., J. O. Obi, …, G. A. Snyder. 2023. The structure of NAD^+ consuming protein Acinetobacter baumannii TIR domain shows unique kinetics and conformations. *J. Biol. Chem.* 299:105290.

84. Fields, J. K., E. J. Gyllenbäck, …, E. J. Sundberg. 2024. Antibodies targeting the shared cytokine receptor IL-1 receptor accessory protein invoke distinct mechanisms to block all cytokine signaling. *Cell Rep.* 43:114099.

85. Wang, Y., H. Yu, …, M. Huang. 2013. Structural Mechanism of Ring-opening Reaction of Glucose by Human Serum Albumin. *J. Biol. Chem.* 288:15980–15987.

86. Abraham, M. J., T. Murtola, …, E. Lindahl. 2015. GROMACS: High performance molecular simulations through multi-level parallelism from laptops to supercomputers. *SoftwareX.* 1–2:19–25.

87. Lakkaraju, S. K., E. P. Raman, …, A. D. MacKerell. 2014. Sampling of Organic Solutes in Aqueous and Heterogeneous Environments Using Oscillating Excess Chemical Potentials in Grand Canonical-like Monte Carlo-Molecular Dynamics Simulations. *J. Chem. Theor. Comput.* 10:2281–2290.

88. Gowers, R., M. Linke, …, O. Beckstein. 2016. MDAnalysis: A Python Package for the Rapid Analysis of Molecular Dynamics Simulations. SciPy Proceedings, pp. 98–105. https://doi.org/10.25080/Majora-629e541a-00e.

89. Michaud-Agrawal, N., E. J. Denning, …, O. Beckstein. 2011. MDAnalysis: A toolkit for the analysis of molecular dynamics simulations. *J. Comput. Chem.* 32:2319–2327.

90. Strickley, R. G., and W. J. Lambert. 2021. A review of Formulations of Commercially Available Antibodies. *J. Pharmaceut. Sci.* 110:2590–2608.e56.

91. Czub, M. P., A. J. Stewart, …, W. Minor. 2022. Organism-specific differences in the binding of ketoprofen to serum albumin. *IUCrJ.* 9:551–561.

92. Ghuman, J., P. A. Zunszain, …, S. Curry. 2005. Structural Basis of the Drug-binding Specificity of Human Serum Albumin. *J. Mol. Biol.* 353:38–52.

93. Ploch-Jankowska, A., D. Pentak, and J. E. Nycz. 2021. A Comprehensive Spectroscopic Analysis of the Ibuprofen Binding with Human Serum Albumin, Part II. *Sci. Pharm.* 89:30.

94. Itoh, T., Y. Saura, …, H. Yamada. 1997. Stereoselectivity and enantiomer-enantiomer interactions in the binding of ibuprofen to human serum albumin. *Chirality.* 9:643–649.

95. Bi, S., L. Yan, …, H. Zhang. 2011. Investigation of ketoprofen binding to human serum albumin by spectral methods. *Spectrochim. Acta Mol. Biomol. Spectrosc.* 78:410–414.

96. Russeva, V., R. Rakovska, …, N. Berova. 1994. Binding of ketoprofen to human serum albumin studied by circular dichroism. *Pharmazie.* 49:519–522.

97. Dufour, C., and O. Dangles. 2005. Flavonoid–serum albumin complexation: determination of binding constants and binding sites by fluorescence spectroscopy. *Biochim. Biophys. Acta.* 1721:164–173.

98. Montero, M. T., J. Estelrich, and O. Valls. 1990. Binding of non-steroidal anti-inflammatory drugs to human serum albumin. *Int. J. Pharm.* 62:21–25.

99. Whitlam, J. B., M. J. Crooks, …, P. V. Pedersen. 1979. Binding of nonsteroidal anti-inflammatory agents to proteins—I. Ibuprofen-serum albumin interaction. *Biochem. Pharmacol.* 28:675–678.

100. Kosa, T., T. Maruyama, and M. Otagiri. 1997. Species differences of serum albumins: I. Drug binding sites. *Pharm. Res.* 14:1607–1612.

101. Evoli, S., D. L. Mobley, …, B. Rizzuti. 2016. Multiple binding modes of ibuprofen in human serum albumin identified by absolute binding free energy calculations. *Phys. Chem. Chem. Phys.* 18:32358–32368.

102. Zhivkova, Z. D., and V. N. Russeva. 1998. Stereoselective binding of ketoprofen enantiomers to human serum albumin studied by high-performance liquid affinity chromatography. *J. Chromatogr. B Biomed. Sci. Appl.* 714:277–283.

103. Yadav, R., and P. Sen. 2013. Mechanistic investigation of domain specific unfolding of human serum albumin and the effect of sucrose. *Protein Sci.* 22:1571–1581.

104. Shil, S., N. Das, …, P. Sen. 2018. Sucrose-Induced Stabilization of Domain-II and Overall Human Serum Albumin against Chemical and Thermal Denaturation. *ACS Omega.* 3:16633–16642.

105. Mazzobre, M. F., M. V. Román, …, H. R. Corti. 2005. Octanol–water partition coefficient of glucose, sucrose, and trehalose. *Carbohydr. Res.* 340:1207–1211.

106. Hansch, C., A. Leo, and D. Hoekman. 1995. Exploring QSAR: Hydrophobic, Electronic, and Steric Constants. American Chemical Society.

107. Pabbathi, A., S. Patra, and A. Samanta. 2013. Structural Transformation of Bovine Serum Albumin Induced by Dimethyl Sulfoxide and Probed by Fluorescence Correlation Spectroscopy and Additional Methods. *ChemPhysChem.* 14:2441–2449.

108. Usacheva, T., G. Gamov, …, V. Sharnin. 2022. Binding of quercetin and curcumin to human serum albumin in aqueous dimethyl sulfoxide and in aqueous ethanol. *J. Therm. Anal. Calorim.* 147:5511–5518.

109. Jayaraj, A., H. A. Schwanz, …, R. Jasuja. 2021. Allosterically Coupled Multisite Binding of Testosterone to Human Serum Albumin. *Endocrinology.* 162:bqaa199.